Quantum Mechanical Modeling of Actinide Complexes: Complexation by Humic Substances and Sorption on Clay Minerals

Abschlussbericht für das Teilprojekt
„Quantenmechanische Modellierung von Aktinoidenkomplexes: Komplexierung durch Huminstoffe und Sorption an Tonmineralen“

im Rahmen des Verbundprojektes
„Wechselwirkung und Transport von Actiniden im natürlichen Tongestein unter Berücksichtigung von Huminstoffen und Tonorganika“

Förderkennzeichen 02E10186

Projektlaufzeit Juli 2006 bis Juni 2011

Notker Rösch, Sven Krüger, Alena Kremleva
Department Chemie, Technische Universität München
85747 Garching

Contents

Das diesem Bericht zugrundeliegende Vorhaben wurde mit Mitteln des Bundesministeriums für Wirtschaft und Arbeit unter dem Förderkennzeichen 02E10186 gefördert. Die Verantwortung für den Inhalt der Veröffentlichung liegt bei den Autoren.

1 Introduction

Migration of actinides is a central topic in the safety analysis of long-term storage of highly radioactive waste. The modeling for predicting the speciation, chemical interactions, and the distribution of actinides in the environment is an important instrument of nuclear waste management as well as of remediation of contaminated sites of uranium mining and former nuclear weapon production. Various chemical and physical processes involving actinides have to be known in some detail as basis of such modeling.

Distribution and transport of actinide elements in the environment are determined by solubility, the versatile aqueous complexation chemistry [1-3], colloid formation and a large variety of solid phases [4,5]. In addition to the chemistry proper of the actinides, under natural conditions one has to take into account also the interaction of aqueous species with other colloids, soils, minerals, and natural organic matter [6,7]. Sorption and colloid formation strongly affect the chemical state as well as the transport behavior of actinide ions. The aquatic chemistry of the more common oxidation states of the early actinides is now fairly well understood [1,3,8]. Much less is known regarding colloid formation, sorption at mineral surfaces, especially for clay minerals, and the interaction with natural organic matter. The latter two topics have been the focus of research of the consortium "Wechselwirkung und Transport von Actiniden im natürlichen Tongestein unter Berücksichtigung von Huminstoffen und Tonorganika". Quantum chemical modeling of actinide chemistry as the central topic of this project has been applied for the first time to the adsorption of actinide ions on clay minerals. Studies of the complexation of actinide ions with organic molecules, which also serve as model functional groups of humic substances, have been extended. These main topics were complemented by the characterization of less well studied actinide species and oxidation states. As a unifying concept, this project complements the experimental studies of the consortium regarding the common goal of improving our knowledge of actinide chemistry at the atomic level, to reach a mechanistic understanding of the essential processes of actinide environmental chemistry.

Two forms of natural organic matter are of concern in this project. On the one hand, humic substances [9], ubiquitous in the geosphere, originate essentially from the degradation of biological materials and are the major organic component of soils, but they also are present in surface and ground waters [9]. The soluble fraction of humic substances, fulvic and humic acids, are composed of very variable organic molecules of varying size and content of functional groups, depending on their origin [9]. They complexate metal ions and are redox active and in this way affect the speciation and the distribution of metals ions in the environment [6,7,9]. Carboxyl groups are considered to be most important for metal, hence also actinide complexation [10-15]. In the previous project it was shown in experimental and computational studies that also alcoholic and phenolic groups contribute to the complexation [16-18]. The possible role of other functional groups is largely unknown.

Experimental efforts to identify and characterize actinide humate complexes mainly rely on extended X-ray absorption fine structure spectroscopy (EXAFS) [19,20] for the determination of average structural parameters. Fourier transform infrared spectroscopy (FT-IR) [21] yields vibrational properties, and time resolved laser fluorescence (TRLFS) studies [22,23] are able to characterize the complexation behavior. Computational studies are useful as they provide information complementary to spectroscopic results [24-26]. For this purpose small organic molecules are used as models of pertinent functional groups of humic sustrances. This approach has also been chosen in various experimental studies [27-29], allowing a direct comparison of results. The study of actinide complexation by small organic acids is also relevant to the examination of the role of the second form of natural organic matter examined in this project, clay organic matter. To a considerable fraction, the organic content of clays is composed of small carboxylic acids, larger acidic organic molecules similar to fulvic acids, and kerogen [30,31]. Complexation of actinides with these species as well as the interaction of this organic content with clay minerals modifies the adsorption chemistry of actinides [32-36]

Actinide adsorption on minerals has widely been studied experimentally, applying batch and column experiments as well as spectroscopic methods [37-39]. Macroscopic experiments show that the adsorption depends on the charge of the actinide ion, yielding adsorption at lower pH for higher charged species. Adsorption is further affected by the presence of organic matter or other metal ions [32-36,40]. Spectroscopic methods like EXAFS, TRLFS, and vibrational spectroscopy allow a microscopic view on adsorbed actinide species. Inner- and outer-sphere complexes as well as mono- and polynuclear adsorbates have been identified; all these complexes may even coexist [41,42]. Preferred mineral surface orientations and their structures in contact with aqueous solution are known only in a few cases. Therefore, a microscopic picture of actinide adsorption at mineral surfaces is currently a topic of intense research as such knowledge is a prerequisite for a thorough thermodynamic modeling. In this project we contributed the first systematic studies of actinide adsorption on clay minerals by density functional calculations of periodic slab models [43].

In experimental investigations on the aqueous chemistry and the sorption of actinides one typically has to treat complex natural systems with a set of species present. Hence, special efforts, e.g., variation of pH, concentrations, ionic strength etc. or chemical manipulations, are required to characterize individual species in these complex systems. Quantum chemical studies provide a complementary view on well defined isolated model species and thus useful references, especially for spectroscopic studies. As exemplified in this report, valuable accurate information on structural and vibrational properties can be obtained in this way, complementing the interpretation of experiments. The calculation of

thermodynamic properties of species in solution and at surfaces presents a more challenging task, but also here important qualitative results have been obtained.

2 Tasks of the Project and Prerequisites

This project was devoted to various topics of actinide environmental chemistry as relevant to safety issues of deep geological storage of radioactive waste. A central theme was the interaction of actinide ions with solvated surfaces of clay minerals, a topic pioneered by the work of this project. In addition, complexation of actinide ions with organic and inorganic ligands in aqueous solution was studied. Here organic ligands represent species of low molecular weight, that are present as natural organic matter in clay formations, and they serve as models of functional groups of humic substances. This project also contributed to the understanding of the hydrolysis of common actinide ions and included some evaluation and development of computational methods related to modeling of solvation.

Surfaces of clay minerals have been modeled as periodic slabs, separated by an appropriate amount of space, more than 1 nm wide, to avoid artificial interactions of neighboring slab instances. In this way, three-dimensional periodicity of the model is achieved, allowing application of established methods for calculating the electronic structure of solids. The electronic structure is calculated at the density functional theory (DFT) level. In this project the projector-augmented-wave (PAW) method as implemented in the program VASP (Vienna ab initio simulation package) [44-49] was used throughout. In this method one-electron wave functions are represented by plane waves augmented by local atomic contributions (at the relativistic level if required) [50]; this approach allows an accurate treatment of heavy elements like actinides. Exchange-correlation potentials of the local density approximation (LDA) and the generalized-gradient approximation (GGA) type [51] have been applied. While LDA in general yields accurate geometries, it overestimates binding energies, especially for weak interactions like hydrogen bonds [51,52]. GGA tends to overestimate bond lengths of heavy-element compounds, but provides considerably improved binding energies [51,52]. Thus, some geometry optimizations were carried out with the LDA functional (as suggested by Perdew and Zunger [53]), while energies and optimizations involving relatively weakly bound water molecules were determined at the GGA level, using the functional suggested by Perdew and Wang (PW91) [54]. Solvation effects on mineral surfaces and adsorption complexes were described by adding the first solvation shell to adsorbates and, in the same spirit, about a water monolayer to the surface. Although this approach of modeling of adsorption systems is well established in other fields, it was applied for the first time by us for the adsorption of actinide species on mineral surfaces [55].

The second major topic of the project was the characterization of complexes of actinides in aqueous solution. Complexation of actinyl ions by various organic ligands was examined as continuation and extension of the central topic of the previous project, the

modeling of actinyl complexation by humic substances and other natural organic matter. New aspects were the complexation by several functional groups, by N- and S-containing groups, as well as the study of ternary complexes as models of species at about neutral pH conditions. In the later phase of the project, this theme was extended to the mechanism and the temperature dependence of complexation by carboxylic groups. Small organic compounds were used as models of functional groups of humic substances. This approach to the complicated chemistry of humic substances had been applied already in earlier experimental [27-29] and computational [56-58] studies. Besides uranyl(VI) as the prototypical actinyl ion, also An(IV) and Am(III) species were examined as examples of less studied actinide species. As most of the other topics mentioned, the latter task was also inspired by the work of partners in the research consortium.

Electronic structure calculations on actinide complexes in solution were also carried out by means of DFT methods. The accurate relativistic density functional Douglas-Kroll-Hess method [59,60] was employed in its scalar-relativistic form, as implemented in the parallel high-performance software PARAGAUSS [61] which is developed by our group. For geometry optimizations mainly the VWN LDA functional [62] was used, while energies were calculated with the GGA functional according to Becke and Perdew (BP) [63,64], fully selfconsistently or in single point fashion employing LDA geometries. Short-range chemical interactions with the aqueous solvent were modeled by explicitly treating aqua ligands [56,57]. In addition, a polarizable continuum model (PCM) [65] was used to account for long-range (electrostatic) solvation effects.

The work of the present project was divided into three parts:

A Complexes in aqueous solution

- **Ternary carboxylate complexes**
  At environmental pH conditions, hydrolysis and carbonate complexation of actinide ions determines the speciation. Thus, the corresponding complexes and not only the aqua ions of actinides have to be regarded as the educts of complexation reactions with other ligands and also ternary complexes including aqua, hydroxide or carbonate ligands may be formed. In this task, hydroxo and carbonato complexes of actinyl ions were modeled as reference. Ternary complexes with carboxylates as common functional groups of humic substances were also examined.

- **Dicarboxylates**
  Dicarboxylate complexes of actinyl ions are well known from experiment, but had not yet been studied computationally. Compared to monocarboxylates these complexes are more complicated with regard to possible combinations of coordination numbers and ligand binding modes. As models for the actinide complexation by humic substances, these complexes can be regarded either as an actinide ion coordinated by (two) small

humic substance molecules or as adducts of a large flexible humic substance species where two carboxylate groups are involved in the binding. Thus, this task was also intended to contribute to resolving open issues of actinide complexation by humates.

- **Alternative functional groups of humic substances**
  In the preceding project our computational studies, together with experiments of the project partner Helmholtz-Zentrum Dresden-Rossendorf, had shown that phenolic or even aliphatic OH groups of humic substances contribute to complexation [57]. This work was to be extended by combined experimental and computational studies on nitrogen- and sulfur-containing groups for the exemplary case of uranyl(VI). The goal was to help understand modifications in the complexation behavior of humic substances of varying chemical composition.

- **Temperature dependence and reaction mechanism of carboxylate complexation**
  The complexation of actinyl ions by simple organic ligands, e.g., acetate, had already been explored in the preceding project. This task was to be extended to more involved topics, such as the mechanism of complexation in aqueous solution and the temperature dependence of corresponding thermodynamic parameters.

- **An(IV) complexes**
  Due to their large formal charge, An(IV) ions represent a challenge for quantum chemical modeling of the corresponding complexes in an aqueous solution. In this task a combined modeling and method development effort was to be undertaken to make An(IV) species accessible to accurate computational treatment. Starting with aqua ions, hydrolysis complexes were treated, ultimately aiming at more complex species. Also experimentally, the oxidation state (IV) of U and Np is less well characterized compared to the more common oxidation states and the results of this task were intended to help augmenting such knowledge.

- **Complexation of Am(III)**
  Experimental as well as computational studies on americium are rare. In this task, the Am(III) aqua ion as well as Am(III) complexes with organic ligands were to be explored in collaboration with the project partner TU Dresden, to contribute to the understanding of the aqueous chemistry of this most stable oxidation state of Am.

B Surfaces of clay minerals and adsorbed complexes

- **Clay mineral surfaces**
  As a prerequisite of adsorption studies, basal and edge surfaces of clay minerals were characterized with respect to their termination, functional groups, and interaction with aqueous solution. Kaolinite, pyrophyllite, and substituted pyrophyllite as a model of clay minerals with charged layers were examined.

- **Adsorption of actinyl on kaolinite**
  Adsorption of actinyl ions on kaolinite were studied as an exemplary system of actinide adsorption on the surfaces of clay minerals, complementing parallel experimental work of the project partners. Inner- and outer-sphere adsorption complexes were compared; various adsorption sites of different protonation state were studied for inner-sphere adsorption. Geometric and energetic results were compared to experimental findings for kaolinite and other clay and related minerals.

- **Adsorption of actinyl complexes**
  Near neutral pH conditions, not only solvated actinyl ions but also various hydroxide or carbonate complexes may interact with clay mineral surfaces, hence were to be characterized as adsorbates, for the exemplary case of uranyl. The results of this task are useful for differentiating various surface species in experiment.

- **Adsorption of actinyl at 2:1 clay minerals**
  As examples of the common 2:1 clay minerals, neutral pyrophyllite and a substituted model mineral with charged layers, similar to beidellite, were studied as substrates for actinyl adsorption. Here the focus was on the edge surfaces as the basal siloxane terminated surfaces are less reactive. Results were compared to those for kaolinite to provide first insight into the variability of actinide adsorption on various clay mineral surfaces.

C Method development

PCM as well as QM/MM and dynamical approaches to model solvation were explored in this task to evaluate their potential for the project.

A technical prerequisite for the large number of demanding calculations carried out in this project was the application of efficient high-performance software for computers with parallel architecture. Complexes in solution were described with the parallel density functional package PARAGAUSS [61], developed in our group and available on a local Linux cluster as well as at the high-performance facilities of Leibniz-Rechenzentrum München. Periodic slab model calculations as models of mineral surfaces have been treated using the PAW approach as implemented in the parallel density functional software VASP which also was used on local as well as central high-performance facilities. The Linux cluster of the group, used for carrying out the work of the project, currently comprises about 160 cores. This local resource was essential for the timely delivery and the overall success of the project. Six dedicated two-processor two-core nodes as well as a stronger four-processor two-core node had been granted which had been put into operation shortly after the start of the project.

3 Development of the State of the Art

Quantum chemical modeling of the chemistry of actinides under environmental conditions is a rather difficult task as several challenges have to be met [25,26,43,66]. The electronic structure of the actinides requires a relativistic treatment including accurate consideration of electron correlation as these elements are very heavy and the three valence shells 5f, 6d, and 7s are involved in bonding. For environmental actinide chemistry modeling the interaction with water as ubiquitous solvent and the surfaces of minerals in contact with an aqueous phase represent yet another challenge.

The electronic structure of solvated complexes is commonly described with a density functional approach, using either gradient-corrected or hydbrid exchange-correlation functionals [66]. Wave function based correlated methods of similar quality like Møller-Plesset perturbation theory [25,67] are also used whereas accurate approaches, e.g., complete active space or coupled cluster methods, are rarely applied and only to smaller complexes in view of their computational demand [68]. Relativistic effects are most easily accounted for by replacing core electrons with an effective core potential [69-71] which allows a nonrelativistic treatment of the valence electronic structure. Direct relativistic all-electron methods, like the Douglas-Kroll-Hess approach [59,60] used in this work or the ZORA (zeroth-order regular approximation) approach [72-74], are computationally more demanding, hence less frequently applied to actinide species in solution. Scalar relativistic as well as spin-orbit interaction including variants of these methods are available [60]. Spin-orbit interaction is especially important for the calculation of electronic spectra [74,75] and accurate thermodynamic properties [76] as well as for oxidation and reduction reactions [66]. On the other hand, it had been demonstrated that spin-orbit effects on geometries and reaction energies of species with only a few f electrons are small [77-79].

Two approaches are available to treat solvation effects on actinide complexes in solution, embedding of the complex in a polarizable continuum model (PCM) [80,81] of bulk water or an explicit molecular treatment of the aqueous solvation environment. The latter method requires a dynamical approach in combination with periodic boundary conditions [82]. When applying the PCM method explicit inclusion of the first solvation shell into the quantum mechanically treated part of the system is mandatory and has been established as standard procedure [25,73,83]. Especially for charged complexes also the chemical interaction with the second solvation shell may be important [84-86], e.g. due to charge transfer, not covered in the PCM approach. Parameters of PCM models have to be chosen carefully to achieve reliable results [84,86,87]. An explicit dynamical treatment of solvation of actinide complexes with a Car-Parinello molecular dynamics approach [88] was presented for some uranyl(VI) complexes and their reactions [82,89] as well as for the solvated Cm(III) ion [90]. As these calculations are quite demanding, they are typically restricted to periodic boxes that include 50–100 water molecules, representing 0.5–1 M

solutions. Thus, in dynamical simulations of more complex and larger systems, empirical force fields are typically applied instead of quantum mechanics [82,91]. An appealing but methodologically intricate intermediate approach is represented by a coupled quantum mechanical and molecular mechanical (QM/MM) model [90,92] where a complex and its immediate solvation environment are treated quantum mechanically, embedded in a larger amount of water molecules that are treated at the force field level. The challenge of this approach, which has already been applied to various types of chemical systems [93-95], is a consistent coupling between the QM and MM parts, especially for water as a solvent. Moreover, due to the dynamics of the aqueous solution a clear separation of the QM and MM parts is not given [96] and has to be introduced as an approximation. Also, the choice of the size of both regions matters. For $[UO_2F_4(H_2O)_n]^{2-}$ it was shown that the experimentally determined five-fold coordination of uranyl could be reproduced only with an explicit QM model of the first solvation shell of 11 aqua molecules [97].

Thus far most computational studies on actinide complexes in solution still address uranium [25,26,66] which is the most commonly studied actinide. In the last years also other actinides have been treated (see Section 4.1.4-6). The computational approaches mentioned above are also applicable to various oxidation states of the early actinides up to Cm. Some noteworthy examples are mentioned in the following. The hydrolysis of Pa(V) has been studied with a dynamical density functional approach showing a variety of oxo and hydroxo complexes to be stable in aqueous solution [98]. In a study of Th(IV) hydrolysis, dimeric complexes have been shown to be stable, in agreement with experimental evidence [99]. Structure calculations on Np(VII) hydroxo and carbonato complexes supported the experimental identification of the Np(VII) tetraoxo dihydroxo species in basic solutions in the presence of carbonate [100]. Pu(IV) and Pu(VI) nitrate and chloro complexes were characterized with GGA density functional calculations [101], achieving good agreement with experiment. The expected similarity of oxidation state (VI) complexes to Np and U congeners was confirmed computationally [101]. The Cm(III) aqua ion was modeled dynamically with quantum mechanical and QM/MM approaches [90]. The coordination number of Cm was determined as 8 with the expected square anti-prismatic structure of the first solvation shell. The calculated structure agreed with results of EXAFS experiments [90].

Quantum chemical modeling of actinide adsorption at mineral surfaces is an emerging field that developed essentially during the time of this project [43,102]. The first studies of this type were published in 2006 [103,104], one by our group. In most studies, periodic slab models combined with a plane-wave approach were used to represent the mineral surfaces [105-108], but also (finite) cluster models were applied [110-113]. These latter models have the advantage to admit a straightforward treatment of charged systems, facilitating the calculation of adsorption energies, at the price of unphysical boundary conditions. In almost

all studies density functional theory was chosen for calculating electronic structures, with the exception of a cluster study on Cm adsorption on corundum where also the MP2 approach was applied to account for correlation [112]. As for complexes in solution, the most frequently studied actinide adsorbate is uranyl(VI). Adsorption of uranyl on corundum [103,113], gibbsite [108,111], kaolinite [43,105-107], titanium dioxide [104], goethite [110], and hematite [114] has been examined so far. In agreement with experimental hints at neutral and higher pH, preferentially bidentate inner-sphere uranyl complexes were modeled. On the other hand, adsorption of hydrolysis species and surface precipitation as well as adsorption of uranyl complexes with various ligands can occur. Here only three studies are available which treated uranyl hydroxide [107,113] and uranyl dimer complexes [111] as adsorbates. The only other actinides for which adsorption on mineral surfaces has been studied quantum mechanically are Np(V) [115] and Cm(III) [112].

An important aspect when modeling actinide adsorption on mineral surfaces is the treatment of solvation. In early studies only the first solvation shell of the actinide ion was taken into account. As the structure and properties of mineral surfaces are modified due to solvation [107,116,117], an explicit (molecular) description of the solvent is necessary. Thus, as a simple solvation model, some studies added a few water molecules to the model [108,109], up to about a monolayer [106,107,110,112] above the mineral surfaces. This approach excludes long-range solvation effects. As a large number of explicit water molecules leads to a potential energy surface of the model system with many close lying minima, a dynamic treatment is necessary when this more realistic solvation treatment is carried out in periodic slab surface models. This computationally rather costly approach has already been chosen for the examination of solvated mineral surfaces [116,118], but has not yet been applied to actinide adsorption on them. The authors plan such studies in the subsequent project.

4 Results

In this section we review the main results of the project; we will follow the project plan. First we present computational results for various actinide complexes in aqueous solution. Then we describe studies on the surfaces of clay minerals and actinyl adsorption thereon. A section on pertinent method development completes this report. Where publications are already available, the presentation will be more concise. Publications resulting from this project are included among the references and also listed in Section 6.

4.1 Actinide complexation in aqueous solution

4.1.1 Hydrolysis and ternary complexes

Uranyl monohydroxide

Uranyl monohydroxide has been studied as this hydrolysis species of U(VI) is one of the less characterized hydrolysis species of uranyl [119]; it is of importance as a reference

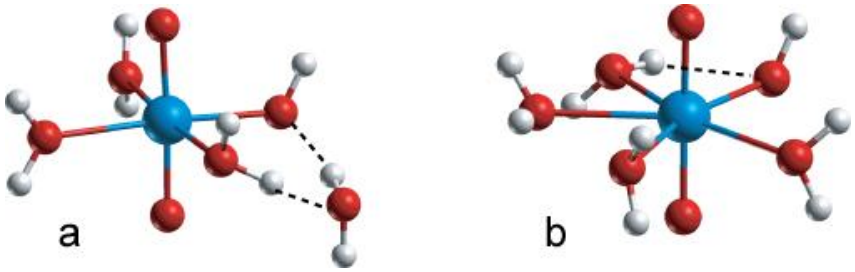

Figure 1. Structure of solvated uranyl monohydroxide $[UO_2OH(H_2O)_4]^+$. (a) Isomer 1, coordination number four. (b) Isomer 2, coordination number five

species for ternary uranyl hydroxo complexes in solution and at mineral surfaces (see below). Uranyl monohydroxide is the simplest hydrolysis product of uranyl(VI) in aqueous solution. Few data are available for $[UO_2OH]^+$ although uranyl hydrolysis has been extensively studied [120]. Experimentally this species is not easily accessible as it appears as a major species only at low uranium concentrations and in a narrow pH interval above pH 3 [121]. At larger uranium concentrations and higher pH values, mononuclear complexes with more than a single hydoxide ligand or polynuclear hydrolysis species dominate [122-124]. Earlier computational studies characterized $[UO_2OH]^+$ as a five coordinate species in aqueous solution [125-130]. Most computational studies produced a bent geometry for the OH ligand (relative to the U-O direction). Computational results in the literature for the Gibbs free energy of hydrolysis ranged from -1.3 kJ mol^{-1} [130] to 55 kJ mol^{-1} [125].

In our model calculations, $[UO_2OH]^+$ species were generated by deprotonation of $[UO_2(H_2O)_5]^{2+}$ at various positions, assuming the typical five-coordination of uranyl. Subsequent geometry optimization for complexes in solution then lead to 7 structural isomers of the model complex $[UO_2OH(H_2O)_4]^+$. These isomers differ in the structure of the hydrogen bonds between aqua and hydroxide ligands. For the isomer labeled as 1, an aqua ligand moved to a position in the second solvation shell. Thus, this isomer corresponds to a four-coordinate species. The relative stability of all these isomers was characterized by abstraction of an aqua ligand, thus referring to $[UO_2OH(H_2O)_3]^+$ as a common reference species. Reaction energies as well as Gibbs free energies (Table 1) show that the four-coordinate isomer 1 is by 7–15 kJ mol^{-1} more stable than the five-coordinate structures. Interestingly, this result is independent of the density functional approach applied, as it was qualitatively confirmed by calculations at the LDA level of theory and by two GGA variants. The geometries of all calculated isomers of uranyl monohydroxide are rather similar (Table 1). Five-coordinated species feature an uranyl bond of 180 pm, a bond to the hydroxide ligand U-O_H = 210–212 pm, and an average equatorial bond length U-O_{eq} of 237–239 pm which was also obtained for various other five-coordinated uranyl(VI) complexes [56-58]. Four-coordinated species show a slightly shorter uranyl bond, 179–180 pm, and, in line with the lower coordination, a lower value of U-O_{eq}, 230 pm. While the

Table 1. Calculated structural parameters of various isomers (VWN, distances in pm), symmetric uranyl stretching frequency ν_s (in cm^{-1}), and Gibbs free energy of aqua ligand abstraction (BP including standard state corrections, in kJ mol^{-1}) of uranyl aqua and uranyl monohydroxide complexes $[UO_2(H_2O)_n(OH)]^+$ with n = 3–4 in aqueous solution.[a]

Complex	isomer	CN	U-O_t[b]	U-O_H	<U-O_W>	U-O_{eq}	ν_s	ΔG_{abs}
$[UO_2(H_2O)_5]^{2+}$		5	177.7	–	237	237	869	
$[UO_2(H_2O)_3(OH)]^+$		4	179.8	209	236	230		
$[UO_2(H_2O)_4(OH)]^+$	1	4	179.3	217	234	230	841	11
	2	5	180.2	212	244	237	830	2
	3	5	180.3	211	244	238	827	1
	4	5	180.3	212	244	237	–[c]	-4
	5	5	180.2	210	245	238	831	2
	6	5	180.3	210	245	237	829	4
	7	5	180.0	210	246	239	834	-1
Exp.								
$[UO_2]^{2+}$ [d]			177(12)		241	241	870[d]	
$[UO_2OH]^+$							849[e]	

(a) Coordination number CN of uranyl, U-O_t – uranyl bond, U-O_H – uranyl-hydroxide bond, <U-O_W> – average uranyl-water bond, U-O_{eq} – average equatorial uranyl-ligand bond. (b) Average values. (c) A numerically reliable result could not be achieved. (d) Ref.[132] (e) Ref. [131].

bond to the hydroxide ligand of the four-coordinate complex $[UO_2OH(H_2O)_4]^+$ is longer, 217 pm, than in the other isomers, the species $[UO_2OH(H_2O)_3]^+$ with U-O_H = 209 pm exhibits a value close to those calculated for five-coordinate uranyl monohydroxide, 210–212 pm (Table 1). The relatively long U-O_H bond of four-coordinate $[UO_2OH(H_2O)_4]^+$ can be traced back to a rather short hydrogen bond between the aqua ligand in the second shell and the OH group (Fig. 1). This result has to be regarded as a special feature of this model; a similar U-O_H bond as shown by all other isomers is expected when the full coordination of the OH ligand by a second shell of water molecules is taken into account in all species.

For uranyl monohydroxide an estimate of the symmetric vibrational frequency of the uranyl unit of 849 cm^{-1} is available [131]. Our calculated results of 841 cm^{-1} for four-coordinated and about 830 cm^{-1} for various five-coordinated uranyl monohydroxide isomers (Table 1) are in favour of the four-coordinated species, in line with the energy considerations (see above). The calculated symmetric vibrational frequency of uranyl of 869 cm^{-1}, in good agreement with the experimental value, 870 cm^{-1} [132], lends further support to our model calculations.

The Gibbs free energy of hydrolysis of the four-coordinated uranyl monohydroxide species is calculated at 23 kJ mol^{-1} (GGA), including standard state corrections. When the

five-coordinated isomers are taken into account via a weighted average according to the Boltzmann distribution, this value is increased by 1 kJ mol^{-1} only. Our computational result agrees reasonably well with the experimental value, 30±1 kJ mol^{-1} [121,133,134], as well as with results of a density functional Car-Parinello molecular dynamic simulation which yielded 34 kJ mol^{-1} for the BLYP GGA, and 21 kJ mol^{-1} for the BP GGA functional [127].

Uranyl monohydroxide served also as an exemplary species to probe effects of self-interaction artefacts in LDA and GGA variants of the Kohn-Sham DF method [135]. The DFT+U approach offers an empirical (partial) correction of such artefacts (see Section 4.3). Strong effects of self-interaction have been identified for the species $[UO_2OH]^+$ in the gas phase. Compared to self-interaction free coupled cluster calculations at the CCSD(T) level, $U\text{-}O_t$ is overestimated by 1 pm with the LDA approach, $U\text{-}O_H$ is underestimated by 2 pm, and the $U\text{-}O_H\text{-}H$ angle is calculated to be linear (180°) instead of 148° [135]. As we showed earlier for uranyl [136], self-interaction weakens the uranyl bond. Due to bond competition, the $U\text{-}O_H$ bond is underestimated. Our analysis demonstrated the rather strong overestimation of the $U\text{-}O_H\text{-}H$ angle to be an indirect effect of artificial uranyl bending and a spurious π-interaction between the OH ligand and the uranyl moiety [135]. These artifacts are essentially corrected with the LDA+U approach, applying a parameter U = 2 eV. Similar effects as for the LDA approach were obtained in GGA calculations [135]. For the modeling of actinide complexes in solution, inspection of the self-interaction effects on fully coordinated complexes is more relevant. As an exemplary case we carried out an analogous calculation on an isomer of $[UO_2OH(H_2O)_4]^+$ in the gas phase [135]. While the direct effects of the weakening of the uranyl bond by 1 pm and the underestimation of the $U\text{-}O_H$ bond by 2 pm are also present in this case, the indirect effect on the $U\text{-}O_H\text{-}H$ angle is strongly damped. For the aqua complex of uranyl monohydroxide this angle is overestimated in a GGA calculations by only 8°. Thus, we conclude that one has to take into account a slight weakening of actinyl bonds and a corresponding underestimation of ligand bond lengths by about 2 pm when comparing conventional LDA and GGA calculations to experiment.

Uranyl hydroxo acetate

The complexation of actinides at environmental pH conditions competes with hydrolysis. Especially for actinides in higher oxidations states like uranyl(VI), which features a rich variety of hydrolysis products, also ternary complexes have been described [137], e.g., with aqua, hydroxide, and carbonate ligands. Therefore, ternary complexes with hydroxide ligands have also been suggested for the complexation with humic substances [21,138-140]. Interestingly, complexation constants for uranyl monohydroxide by humate have been reported to be similar or slightly higher than for uranyl ions by humate [21,138-140]. Similar results have been obtained for Am(III) and Cm(III) [141,142]. As the complexation chemistry of uranyl(VI) in the range of approximately neutral pH is of particular relevance for safety issues of deep geological repositories for radioactive waste, we undertook a study

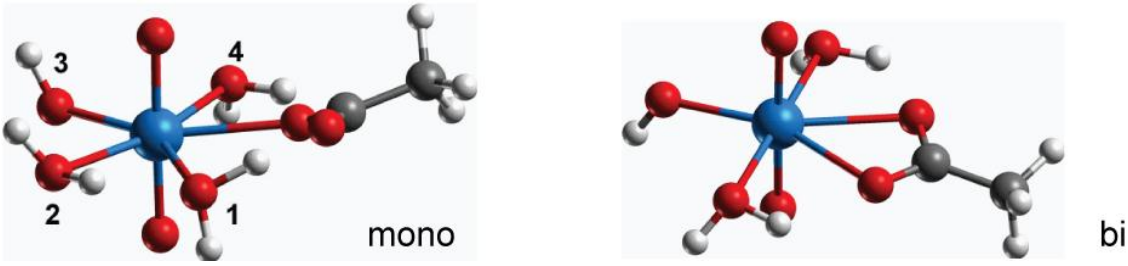

Figure 2. Structure of ternary complexes of uranyl with mono- and bidentate coordinated acetate, a trans-hydroxo moiety, and aqua ligands. Numbers label the various possible positions of the hydroxide ligand.

of ternary uranyl acetate complexes in aqueous solution [143]. These results may also serve as models of carboxylic functional groups of humic substances. Until now structural and vibrational properties of such complexes are only poorly known; therefore, this work provides hints for a direct spectroscopic identification of the corresponding complexes.

Mono- and bidentate acetate coordination of acetate to uranyl monohydroxide at various relative positions of the ligands in the first coordination shell of uranyl have been modeled (Fig. 2). For the monodentate acetate coordination four isomers result, while the local symmetry of the bidentate acetate species reduces the variety of relative ligand positions to two, with the OH ligand in cis or trans position relative the acetate (Fig. 2).

In Table 2, geometric as well as vibrational and energetic characteristics of ternary uranyl hydroxo acetate complexes are compared to their binary uranyl acetate congeners for the more stable trans isomers. Cis isomers of uranyl hydroxo acetate exhibit similar characteristics, but are slightly less stable, as expected due to repulsion of the anionic ligands [143]. As a result of bonding competition, the hydroxide ligand in these ternary complexes induces marked structural changes compared to the binary acetate complexes. The uranyl bond elongates by 2 pm. In line with this weakening of the uranyl bond, the symmetric uranyl stretching frequency is red shifted by about 30 cm^{-1} (Table 2), a value which is rather similar to our result for uranyl monohydroxide (see above). A somewhat smaller red shift was observed in a recent attenuated total reflection (ATR) FT-IR experiment for the asymmetric uranyl vibration in ternary uranyl hydroxo humat complexes compared to uranyl humate [138], by 12 cm^{-1} for uranyl humate solution and about 20 cm^{-1} for uranyl humate solid. U-O bonds to the acetate ligand increase by 7 pm and 13 pm for mono- and bidentate ligand coordination, respectively. In consequence, also the U-C distance to the carbon atom of the acetate ligand increases in case of bidentate coordination, but not for monodentate species where the carboxyl C-O bond decreases. Also the bonds of the aqua ligands to uranyl are elongated, by 7–8 pm (Table 2). In line with earlier findings for other uranyl complexes [56,58], all these changes have no effect on the average equatorial distance U-O_{eq}, which for binary and ternary complexes is calculated in the typical range of 236–238 pm for five-coordinate uranyl(VI) complexes. Once again these

Table 2. Calculated structure parameters[a] (LDA, distances in pm), symmetric uranyl stretching frequency ν_{sym} (in cm^{-1}) as well as Gibbs free energies ΔG_{sub} of ligand substitution (single-point GGA, in kJ mol^{-1}) of uranyl acetate $[UO_2(OOCCH_3)(H_2O_n)]^+$ and uranyl trans-hydroxo acetate complexes $[UO_2(OH)(OOCCH_3)(H_2O_{n-1})]$ with bidentate (bi) and monodentate (mono) coordination (n = 3, 4) in aqueous solution.

Ligand		U-O_t	U-O_C	U-C	U-O_W	U-O_H	U-O_{eq}	ν_{sym}	ΔG_{sub}
bi	$[UO_2]^{2+}$	178.6	237	277	236	–	237	854	-109
	$[UO_2(OH)]^+$	180.6	244	284	244	212	238	820	-69
mono	$[UO_2]^{2+}$	178.9	229	340	238	–	236	822	-110
	$[UO_2(OH)]^+$	180.8	242	341	243	214	237	796	-63

(a) U-O_t – uranyl bond U-O_t, U-O_C – uranium bond to carboxylate, U-C – uranium distance to carboxyl C, U-O_W – yranyl bond to aqua ligand, U-O_H – uranyl-hydroxide bond, U-O_{eq} – average equatorial uranyl-ligand bond.

examples show that the geometric parameter U-O_{eq}, which is commonly determined in EXAFS studies, is not sensitive to the coordination modes or types of ligands. The only key characteristic geometric feature of uranyl hydroxo acetate complexes is the rather short bond of the hydroxide ligand U-O_H, 212–214 pm, which may be used as fingerprint in experimental structure analysis.

The Gibbs free energies of complexation of uranyl monohydroxide with acetate (Table 2) are clearly lower than for uranyl itself; this translates into a lower complexation constant of uranyl monohydroxide. This result can be rationalized by the lower charge of $[UO_2OH]^+$ compared to $[UO_2]^{2+}$. This finding is qualitatively at variance with experimental results for uranyl hydroxo humate species (see above) although the experimentally determined red shift of the uranyl asymmetric vibrational frequency also points to a change in ligand bonding to uranyl comparable with our results. All these results demonstrate that at least at neutral to basic pH conditions the complexation of uranyl by humic substances at the microscopic level deserves further exploration.

Diacetate complexes

Uranyl diacetate species are present in solutions of uranyl and acetate at weakly acidic pH [144] and may serve also as models of uranium complexated by more than one carboxyl group of humic subtances. Two acetate ligands were coordinated to uranyl ion in bidentate/bidentate, bidentate/monodentate, and monodentate/monodentate fashion (Fig. 3) and the first coordination shell was filled up with aqua ligands to reach the common coordination numbers CN = 5 and 6. The 1:1 complexes of acetate with uranyl show very similar Gibbs free energies of complexation for bidentate and monodentate coordinations with the bidentate coordination slightly preferred (Table 3). The various 1:2 uranyl acetate complexes are very close in energies too. Monodentate/monodentate and bidentate/ monodentate coordinations are essentially degenerate, while bidentate/bidentate coordination is about 10 kJ mol^{-1} less favorable (Table 3). The calculated structural

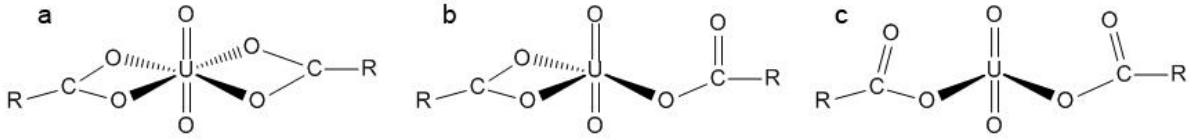

Figure 3. Coordination modes of biacetate complexes $[UO_2(OOCCH_3)_2]^0$: (a) bidentate-bidentate, (b) bidentate-monodentate, (c) monodentate-monodentate.

parameters are rather similar for all three diacetate complexes. The U-O_t bond is 179–180 pm and marginally shorter values are calculated for twofold bidentate ligand coordination as for the monoacetate complex (Table 3). The average U-O_C bond to the acetate ligands amounts to 237-241 pm for all three types of coordination, which is slightly longer than for bidentate monoacetate. An average equatorial distances U-O_{eq} of 236–238 pm is obtained for all five-coordinate species. This geometric parameter depends essentially only on the coordination number (see above) [56,58], as is demonstrated for the six-coordinate bidentate/bidentate diacetate complex with U-O_{eq} = 242 pm. The only structural parameter characteristic for the coordination mode is the U-C distance to the carboxyl group. Its average elongates from about 280 pm for bidentate coordinated complexes to about 330 pm for monodentate species for 1:1 as well as 1:2 complexes (Table 3).

An EXAFS study on uranyl acetate complexation suggests the prevalence of 1:2 complexes at pH 2 to 3.2 [144] and interprets a slight increase in U-O_{eq} with time as a change of the coordination mode from mono- to bidentate. The resolved U-O_t bond of about 179 pm is in good agreement with our calculational results. U-O_{eq} of 242–245 pm is longer

Table 3. Calculated structure parameters[a] (LDA, distances in pm) and Gibbs free energies ΔG_{sub} of ligand substitution (GGA, in kJ mol^{-1}) of uranyl mono- and diacetate $[UO_2(OOCCH_3)_m(H_2O_n)]^0$, m = 1 and 2, with monodentate (mono) and bidentate coordination of ligands in aqueous solution. Experimental results for uranyl diacetate are given for comparison.

Coord.	Ac^-	CN	U-O_t	U-O_C	U-C	U-O_{eq}	ΔG_{sub}
bi	1	5	178.7	237	277	237	-108
mono	1	5	179.0	228	333	236	-107
bi/bi	2	5	179.2	237	277	238	-175
	2	6	179.8	241	280	242	
bi/mono	2	5	179.7	237	305	236	-185
mono/mono	2	5	179.9	238	336	236	-186
EXAFS[b]							
pH 1.8, 3 months			179(2)		294(2.2)	245(4.4)	
pH 1.8			179(2)		292(2.3)	242(4.6)	
pH 3.2			178(2)		292(1.9)	245(3.8)	

(a) Ac^- – number of acetate ligands, CN – coordination number of uranyl, U-O_t – uranyl bond, U-O_C – uranium bond to carboxylate, U-C – uranium distance to carboxyl C, U-O_{eq} – average equatorial uranyl-ligand bond. (b) Ref. 144

than our calculated values for five-coordinate complexes (Table 3) but fits to U-O_{eq} of the bidentate/bidentate diacetate complex with CN = 6 of 242 pm (Table 3). Thus, comparison of EXAFS and calculated results suggests a prevailing coordination of 6, at variance with the lower measured coordination numbers. Also the increase of U-O_{eq} with time may be due to an increase of the average coordination number. The measured U-C distance of 292–294 ± 3 pm, together with a coordination number of ~2, confirming the presence of diacetate complexes, lies between the values calculated for purely mono- or bidentate coordinated diacetate complexes. Thus a mixture of mono- and bidentate coordinated ligands should be present, in agreement with calculated Gibbs free energies of complexation (see above).

4.1.2 Complexation by non-carboxylic groups

To complement ongoing experimental efforts of the project partner Helmholtz-Zentrum Dresden-Rossendorf in characterizing the role and importance of other than carboxylic functional groups in actinide complexation by humic substances, we studied uranyl complexation as an exemplary case with small organic species which exhibit S- and N-related heterogroups as models of analogous functional groups of humic substances.

Complexation by sulfur containing groups

The complexation of uranyl(VI) by a single sulfonate or thiolate ligand was examined as a model of the corresponding functional groups of humic substances [145]. Humic substances typically show a sulfur content of less than 1.5 % [9]. Yet, at environmentally relevant low actinide concentrations, a contribution of such functional groups can be excluded only by demonstrating that their propensity for complexation is less favorable than that of other functional groups. This computational modelling was related to experimental TRLFS studies at Helmholtz-Zentrum Dresden Rossendorf on the complexation by benzenesulfonic acid (BSA) and 4-hydroxybenzenesulfonic acid (HBSA) [145] as well as complexation by sulfur enriched humic acids [146] which mainly feature sulfur in high oxidation state as thiolate groups. An interesting finding of earlier TRLFS studies was that HBSA complexates uranyl while for BSA no complexation could be detected [147]. This a little surprising finding motivated our study together with an experimental reinvestigation of these systems under strictly comparable conditions.

Uranyl complexes in aqueous solution with BSA, HBSA, and also methylsulfonate as ligands have been optimized, assuming five-fold coordination. For comparison also methanethiolate was included in this study. Table 4 collects pertinent geometric parameters of all complexes treated and Gibbs free energies of the model complexation reaction

$$[UO_2(H_2O)_5]^{2+} + L^- \rightarrow [UO_2L(H_2O)_n]^+ + (5–n)\ H_2O \qquad (1)$$

Mono-, bi-, and tridentate coordination of the sulfonate group to uranyl was examined. While optimizations lead to stable structures with mono- and bidentate coordination (Fig. 4), no energetic minimum could be found for tridentate coordination. The uranyl bond length as

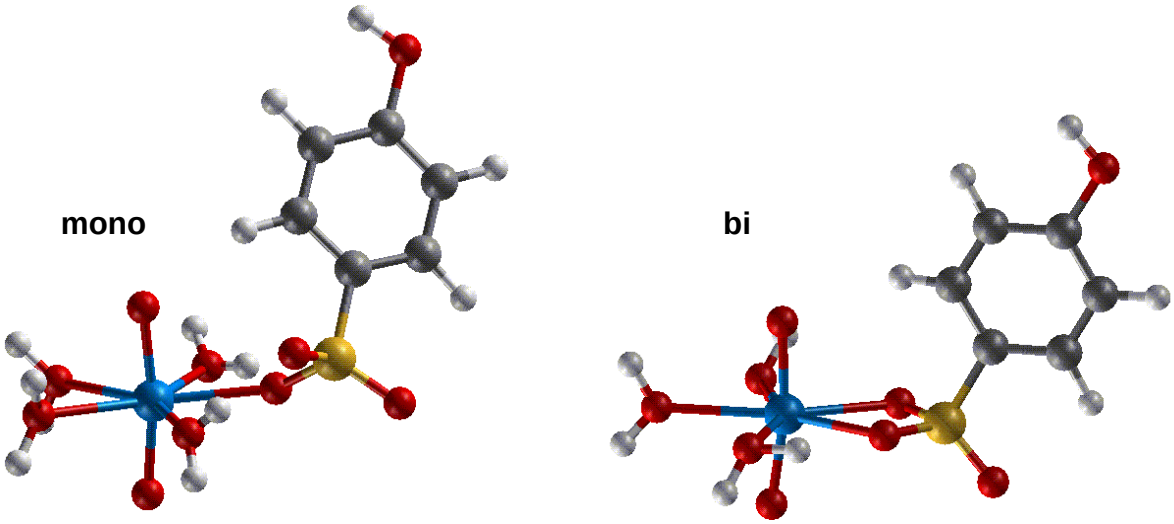

Figure 4. Mono- and bidentate uranyl complexes $[UO_2(C_6H_4OH)SO_3(H_2O)_n]^+$ with an HBSA ligand in aqueous solution.

well as the average equatorial U-O distance U-O_{eq}, the structure parameters commonly determined in EXAFS investigations, are very similar for all three sulfonates and vary only marginally with the coordination mode (Table 4). For monodentate coordination, U-O_t is elongated by less than 0.5 pm and U-O_{eq} is 1–2 pm shorter than for bidentate coordination. These results indicate a slightly stronger uranyl-ligand interaction for monodentate coordination. The weak variation of the distance U-O_{eq} between mono- and bidentate complexes is in line with earlier findings for carboxylates which showed that the value of U-O_{eq} mainly reflects the coordination number, but not the coordination mode [56,148]. The trend of the uranyl-sulfonate bond, tentatively interpreted as stronger for monodentate complexes, is corroborated by the distances U-O_S from uranyl to the sulfonate oxygen centers. For monodentate complexes a short bond of ~230 pm was calculated, while for bidentate coordination two bonds of ~240 pm were determined. Another clear geometric differentiation of the coordination modes is provided by the U-S distances which amount to ~310 pm for bidentate coordination, but to ~360 pm for monodentate species. This geometric feature of uranyl monosulfonate complexes is best suited for a potential differentiation of the coordination mode by EXAFS measurements. With regard to the complexation behaviour of BSA and HBSA, note that the geometric parameters of BSA and HBSA complexes are more similar to each other than to the corresponding methylsulfonate complex.

Comparison of sulfonate complexes to uranyl methanethiolate reveals notable differences in the structure. The uranyl bond U-O_t = 179 pm is up to 1 pm longer than for the sulfonate complexes, pointing towards stronger bonding of the ligand. The bond U-S = 267 pm is clearly much shorter than the U-S values of sulfonate complexes. Averaging jointly over the equatorial distances U-O and U-S yields a value of 247 pm, considerably larger than the value U-O_{eq} of ~237 pm calculated for five-coordinate uranyl sulfonate or

Table 4. Calculated distances[a] (pm) of mono- and bidentate uranyl(VI) sulfonate $[UO_2L(H_2O)_n]^+$, L = RSO_3^-, and thiolate, L = RS^-, with n = 4 for monodentate and n = 3 for bidentate complexes. Results for the complexes with the acetate ligand, L = $[CH_3COO]^-$, are given for comparison. Gibbs free energies ΔG_{sub} (single-point BP, kJ mol^{-1}) including standard state corrections are estimated according Eq. (1).

Ligand	coord. mode	R	U-O_t	U-$O_{S/C}$	U-S/C	U-O_{eq}	ΔG_{sub}
RSO_3^-	mono	CH_3	178.7	229	354	237	-35
		C_6H_5	178.7	232	362	236	-27
		C_6H_4OH	178.7	231	361	236	-26
	bi	CH_3	178.3	240, 242	306	238	-32
		C_6H_5	178.4	240, 243	308	238	-26
		C_6H_4OH	178.6	240, 242	307	238	-23
RS^-		CH_3	179.3	–	267	247	-75
$RCOO^-$	mono	CH_3	178.9	229	340	236	-105
	bi	CH_3	178.6	237, 237	277	237	-108

(a) U-O_t – average terminal uranyl bond, U-$O_{S/C}$ – bond to oxygen centers of the sulfur-containing or carboxylic ligand L, U-S/C – distances to the S/C center of L, U-O_{eq} – average equatorial U-O/S bond.

acetate complexes (Table 4). Thus, this quantity is a simple geometric feature for identifying thiolate complexes by means of EXAFS.

Gibbs free energies of sulfonate complexation calculated according to the model equation (1) yield only small differences, of up to 3 kJ mol^{-1}, between complexes with BSA and HBSA ligands. Thus, one expects that both acids show a very similar complexation behaviour for uranyl, as confirmed by very recent TRLFS experiments of the project partner Helmholtz-Zentrum Dresden-Rossendorf. In these spectroscopic measurements, the complexation constant of uranyl complexation with BSA and HBSA were determined at 2.62 and 2.67, respectively [145]. Interestingly, these values are rather close to the complexation constants measured for uranyl monoacetate, 2.5–2.9 [149-151]. This similarity is at variance with the calculated Gibbs free energies of complexation: -20 kJ mol^{-1} to -35 kJ mol^{-1} for sulfonate complexation, but more exothermic, -105 kJ mol^{-1} for mono-, and -108 kJ mol^{-1} for bidentate coordination of acetate. Recall that complexation constants of organic acids have been shown to correlate with the corresponding pK_a values [152].

The higher pK_a value of acetic acid, 4.76, is reflected by our calculated results, but not by the experimental complexation constants for acetate and sulfonate ligands which feature pK_a values below zero [153]. Thus, the measured unexpectedly high complexation constants of sulfonates, at variance with general trends [152] and our computational results, represent an open problem, to be examined in more detail. Note that an earlier finding of a rather high

Table 5. Gibbs free energies ΔG_{sub} (single-point BP) of ligand substitution for complexes $[UO_2(H_2O)_4L_N]^{2+}$, L_N = NH_2Me, NMe_3, and NC_5H_5, in solution, optimized without constraints. Results for complexes with neutral ligands L = CH_3OH, C_6H_5OH, and CH_3COOH, as well as the anionic ligand CH_3COO^- are given for comparison. Free energies ΔG^H_{sub} of complexation with protonated ligands L_NH^+ or neutral ligands LH. All energies in kJ mol^{-1}.

		ΔG_{sub}	ΔG^H_{sub}
L_N	NH_2CH_3	-9	120
	$N(CH_3)_3$	39	158
	NC_5H_5	13	111
L	CH_3OH	8	28
	C_6H_5OH	57	57
	CH_3COOH	20	33
	CH_3COO^- mono	-109	
	CH_3COO^- bi	-110	

complexation constant, at variance with the correlation with pK_a, had been rationalized by the coexistence of inner- and outer-sphere complexes [152].

Complexation by nitrogen containing groups

Just as sulfur, nitrogen is also a smaller component, reaching up to ~4 %, in the elemental composition of humic substances [9]. Nitrogen appears in various functional groups, e.g., in amines and amides, as well as in amino, imino, and heterocyclic moieties. While multidentate nitrogen donor ligands are common in separation chemistry [154,155], such complexating units are not to be expected in humic substances. Thus, we examined amines, pyridine, and amino acids [156,157] as models of more probable N-donor functional groups of humic substances. Especially amino acid groups may be of interest as they allow chelate complexation of metal ions.

Structural parameters for uranyl complexes with methylamine, trimethylamine, and pyridine, like the uranyl bond and bonds to aqua ligands, are similar to monocarboxylate complexes [156]. U-N bonds of ~248 pm are a characteristic feature, as they are longer than U-O bonds of carboxyl complexes (229 pm monodentate, 237 pm bidentate, see above). This relationship reflects the larger size of the N atom compared to O. Consequently, the average equatorial U-O/N distance, which is often measured by EXAFS, elongates by 2 pm [156] compared to uranyl monoacetate.

Table 5 compares Gibbs free energies ΔG_{sub} of complexation with neutral N-donor ligands or with their conjugate cationic acids (ΔG^H_{sub}) according to the reaction

$$[UO_2(H_2O)_5]^{2+} + L_N \rightarrow [UO_2(H_2O)_4L_N]^{2+} + H_2O \quad (2)$$

Table 6. Geometry parameters[a] (in pm) and Gibbs free energies ΔG_{sub} (single-point BP, in kJ mol^{-1}) of ligand substitution for complexes $[UO_2L(H_2O)_3]^{0,+}$ of uranyl with the α-amino-isobutyric acid anion AIB and the neutral acid AIBH. For comparison also results for the carboxylates with acetate, benzoate, salicylate, and glycolate and given. Bidentate (bi) and chelate coordination of the ligand are compared.

Coord.	Ligand	U-O_t	U-O_C	U-N/O	U-C	U-O_W	U-O_{eq}	ΔG_{sub}
bi.	acetate	179	237		277	237	237	-110
	benzoate	179	237		277	236	237	-98
	salicylate	178	237		277	237	237	-61
	glycolate	178	239		277	235	237	-78
	AIB cis	179	237		276	239	238	-82
	AIB trans	179	237		276	237	237	-88
	AIBH	178	241		277	235	237	-59
chelate	salicylate	179	218	246	341	240	237	-49
	glycolate	179	223	244	326	238	236	-82
	AIB	179	226	248	325	237	238	-118

(a) U-O_t – average uranyl bond, U-O_C – uranium bond to carboxylate, U-N/O – uranium bond to N or O centers of chelating ligands, U-C – uranium distance to carboxyl C, U-O_W – yranyl bond to aqua ligand, U-O_{eq} – average equatorial uranyl-ligand bond.

to results for methanol, phenol, and acetic acid. Neutral amines and pyridine show low complexation energies, comparable to those calculated for neutral OH functional groups. While methylamine complexates slightly stronger than an aqua ligand, G_{sub} = -9 kJ mol^{-1}, trimethylamine yields an endothermic complexation energy of 39 kJ mol^{-1} due to its larger steric demand. As neutral amine or pyridine groups are present at about neutral or higher pH, no sizeable contribution to actinide complexation in humic substances is expected because at these conditions the prevailing carboxyl groups are deprotonated. Also at low pH, where these groups acquire their cationic acid form, alcoholic, phenolic and neutral carboxyl groups form more favorable complexation sites, as is demonstrated by the much higher endothermic ΔG^{H}_{sub} values calculated for the N-donor ligands (Table 5) [156].

The complexation of uranyl by amino acids was studied in exploratory fashion on the examples glycine, alanine, and α-amino-isobutyric acid (AIB) [157]. The latter model ligand was treated in more detail as a corresponding EXAFS study is available [27]. Bidentate and chelate coordination of the amino acid group may be invoked as favorable coordination modes of the ligand. For bidentate coordination U-O bonds to the carboxyl group and to aqua ligands in general are rather similar (Table 6). Neutral AIB is an exception where the average U-O_C distance to the carboxyl group, 241 pm, is by 6 pm longer than the bonds to aqua ligands. Also, the geometric features of isomers (cis and trans orientation of the N lone pair with respect to the carboxyl group) of bidentate coordinated AIB and other carboxylic

acids are very similar (Table 6). Chelate complexes are easily distinguishable geometrically from their bidentate congeners. The single bond U-O_C is by more than 10 pm shorter and the bonds to the amine group or the hydroxyl ligand in case of carboxylic acids, 244–248 pm, are longer than typical U-O_C distances of bidentate complexes, 237–241 pm (Table 6). A marked difference between bidentate and chelate coordination, useful for identification by means of EXAFS, is the U-C distance. It is calculated to ~277 pm for bidentate coordination of AIB and to 325 pm for the corresponding chelate complexes. Similar results were obtained for salycilate and glycolate complexes (Table 6).

Comparison of energy parameters for bidentate and chelate complexes of uranyl with the three exemplary amino acids shows that for the neutral form of the acids bidentate complexation is preferred by about 45 kJ mol^{-1}, while the anionic form of the ligand is more stable in chelate complexes, by 20–30 kJ mol^{-1}. Thus bidentate coordination is expected at acidic pH, while chelate complexes should appear in the basic regime, in agreement with experimental results [27]. Chelate complexes of carboxylic acids show a free energy of complexation that is lower or comparable to bidentate complexes, but the uranyl AIB chelate complex shows the highest endothermic complexation energy among all examples studied (Table 6). Thus, at lower to neutral pH where amino acids are protonated, carboxyl groups are preferred for uranyl complexation. On the other hand, at basic pH conditions, amino acid moieties offer more favorable sites for complexation via the formation of chelate complexes. Taking into account the low nitrogen content of humic substances, only a slight increase of the complexating ability is thus expected, due to amino acid groups, at high pH conditions.

4.1.3 Carboxylate complexation: Effect of temperature and mechanism

Temperature dependency of uranyl acetate complexation

The majority of actinide complexation studies were carried out at room temperature. Only few data are available at elevated temperatures [28,158] that are of interest when modelling chemical processes for safety issues of deep geological storage sites where temperatures of 100°C and above have to be considered in the near field.

The hydrolysis of uranyl(VI) was studied experimentally in the temperature range from 10 to 94 °C [159-161]. In that temperature interval hydrolysis of uranyl proceeds as formation of $[UO_2OH]^+$, $[(UO_2)_2(OH)_2]^{2+}$, and $[(UO_2)_3(OH)_5]^+$ in acidic solutions, and all three hydrolysis constants increase with temperature, but to a different degree [161]. Therefore, the speciation of U(VI) varies with temperature T.

Several experimental studies examined the complexation of uranyl with carboxylates at elevated temperature [28,162-164]. Titration calorimetry was used to determine the enthalpy of complexation from 10 to 85 °C. The complexation of uranyl with acetate, malonate, oxydiacetate, and thiodiacetate is always endothermic and driven by entropy. The

enthalpy and entropy of complexation both become more positive at higher T. The complexes are stabilized at higher T as the increase of the entropy term TΔS exceeds the enthalpy change. Similar thermodynamic trends have been observed for the complexation of carboxylates with other actinide and lanthanide cations, including Th(IV) [165], Nd(III) [166], and Sm(III) [162].

To inspect the microscopic origins of these findings, we examined uranyl acetate complexes at 25, 50, 75, and 90 °C. Monodentate and bidentate 1:1 and 1:2 uranyl complexes with acetate were optimized in the gas phase and in solution, applying the BP functional. Thermodynamic corrections of the energy values, to determine enthalpy and entropy terms, were first calculated from a normal mode analysis in the gas phase. The temperature dependence of solvation effects was modelled via the temperature variation of the dielectric constant $\varepsilon(H_2O)$ of water [167,168] and the cavitation energy [169]. The values $\varepsilon(H_2O)$ = 78.4, 69.9, 61.5, and 56.3 at 25 °C, 50 °C, 75 °C, and 90 °C as derived from [167] were used. The Gibbs free energy ΔG_{aq} of complexation reactions in solution was estimated by invoking a thermodynamic cycle that involves the Gibbs free energy ΔG_{gas} in the gas phase, adding for each species its Gibbs free energy ΔG_{sol} of solvation. Reaction free energies were adjusted to the standard concentration of 1 M for solutes ($\Delta G_{st}(T)$ = 7.91, 8.57, 9.23, and 9.63 kJ mol^{-1} for T = 25 °C, 50 °C, 75 °C, and 90 °C, respectively) and to the standard concentration of water, 55.34 M ($\Delta G_{st}(T)$ = 17.85, 19.34, 20.83, and 21.73 kJ mol^{-1} at T = 25, 50, 75, and 90ºC, respectively) for each solvated water molecule.

To examine the effect of temperature on the uranyl complexation by acetate we studied the model reactions

$$[UO_2(H_2O)_5]^{2+} + Ac^- \rightarrow [UO_2(H_2O)_{5-n}Ac]^+ + n\ H_2O \quad (3)$$

$$[UO_2(H_2O)_5]^{2+} + AcH \rightarrow [UO_2(H_2O)_{5-n}Ac]^+ + [H_3O]^+ + (n\text{-}1)\ H_2O \quad (4)$$

$$[UO_2(H_2O)_5]^{2+} + AcH \rightarrow [UO_2(H_2O)_{5-n}Ac]^+ + [H_5O]^+ + (n\text{-}2)\ H_2O \quad (5)$$

$$[UO_2(H_2O)_5]^{2+} + AcH \rightarrow [UO_2(H_2O)_{5-n}Ac]^+ + [H]^+_{exp} + n\ H_2O \quad (6)$$

for monodentate (n = 1) and bidentate (n = 2) ligand coordination.

Equation (3) models the standard equation of metal complex formation, but has the disadvantage of including cations as well as anions. As inaccuracies of a PCM method are particularly pronounced for charged species and commonly larger for anions [170,171], it is computationally favourable to use Eqs. (4–6) because they comprise only cations and thus tend to afford a more favourable error compensation. From Gibbs free energies determined according to Eqs. (4–6), corresponding values of Eq. (3) can be derived with the Gibbs free energy of deprotonation of acetic acid. Here the experimental value of the pK_a of acetic acid at normal conditions (4.59±0.01), which increases with temperature to 4.72 at 70 °C, can be used [28]. In Eq. (4) the solvated proton is modelled as H_3O^+, in Eq. (5) as Zundel ion, while

Table 7. Thermodynamic parameters of uranyl(VI) monoacetate complexation with mono- and bidentate coordination for various temperatures as calculated from Eq. (3) in the gas phase (g) and in solution (s) at the GGA level as well as with standard state corrections (st).

	$\Delta E(s)$	$\Delta H_{st}(g)$	$-\Delta(ST)(g)$	$\Delta G_{st}(s)$	log β
mono					
25	-125.3	-117.2	10.2	-107.0	18.8
50	-127.1	-118.2	11.1	-107.1	17.4
75	-129.3	-119.6	12.0	-107.6	16.2
90	-130.9	-120.7	12.5	-108.2	15.6
bi					
25	-90.6	-70.1	-38.1	-108.2	19.0
50	-91.6	-68.9	-41.3	-110.1	17.9
75	-93.0	-67.9	-44.4	-112.4	16.9
90	-94.0	-67.6	-46.3	-113.9	16.4

in Eq. (6) the value of 1105 kJ mol^{-1} is used for the solvation energy of the proton as obtained in a systematic ion cluster-pair study [172] (in agreement with experimental data).

Table 7 provides the Gibbs free energies estimated according to Eq. (3) for 1:1 uranyl mono- and bidentate complexes with acetate. The experimental value ΔG of the 1:1 complex formation was measured at -15 kJ mol^{-1} at room temperature [28]; it decreases slightly with increasing temperature. At 70 °C, ΔG amounts to -20 kJ mol^{-1} [28]. As a result, the corresponding complexation constant increases from 2.61±0.03 to 3.01±0.05 when T increases from 25 °C to 70 °C [28]. An U-C contact of 290 pm and coordination number 1.3 was resolved at pH 2.84, confirming the presence of inner-sphere 1:1 uranyl complexes with acetate [28].

The calculated data from Eq. (3) do not fit the experiment (Table 7). The free energy change of the reaction, about -110 kJ mol^{-1} at 25 °C, considerably overestimates (in absolute terms) the experiment, resulting in too large a complexation constant of ~19 (Table 7). This failure in reproducing the free energy of complexation mainly is to be attributed to shortcomings of the solvation model mentioned above [170,171]. Much better results were obtained for the trend with increasing temperature. The monodentate complex is marginally less stable than the bidentate one and that difference becomes larger with T, rendering bidentate coordination increasingly more favourable. Going from 25 °C to 75 °C, ΔG decreases by 1 kJ mol^{-1} for monodentate complexes and 4 kJ mol^{-1} for bidentate complexes. The latter value agrees very well with the experimental results, a change by 5 kJ mol^{-1} at 70 °C [28].

Bidentate and monodentate complexes show opposite signs of the gas phase entropy contribution to the Gibbs free energy. The entropy term -TΔS stabilizes the bidentate complex by ~40 kJ mol^{-1}, but slightly destabilizes the monodentate complex by ~10 kJ mol^{-1} (Table 7). This effect can be rationalized by the fact that bidentate coordination implies the

Table 8. Temperature dependence of the Gibbs free energy ΔG (GGA) of uranyl(VI) complexation by an acetate ligand according to model reactions Eqs. (3–6) for mono- and bidentate coordination. Given are values at 25 °C and their change Δ^2G upon temperature increase to 90 °C as well as the difference Δ(bi-mono) of Δ^2G values of mono and bidentate complexes in solution (s) including standard state corrections (st).

	Eq.	3	4	5	6
ΔG_{st}(s, 25)	mono	-107	-3	-57	-36
	bi	-108	-4	-58	-37
$\Delta^2 G_{st}$(s, 90)	mono	-1	-7	-5	-7
	bi	-6	-12	-9	-12
	Δ(bi-mono)	-5	-5	-5	-5

release of one more aqua ligand from the first coordination shell of the uranyl aqua complex than for complexes with monodentate coordination, which lowers the reaction entropy. Experimental results show complexation with acetate to be entropy driven [28]. According to our calculations, this holds only for the bidentate complex.

Using Eqs. (4–6) more realistic Gibbs free energies were calculated for the complexation of uranyl with acetate (Table 8). Eq. (4) yields a marginally exothermic reaction in best agreement with experiment. Modelling the solvated proton as $[H_5O_2]^+$ species again overestimates the Gibbs free energy, leading to a reaction energy of about -60 kJ mol^{-1}, while invoking the experimental solvation energy of a proton provides an intermediate value of the reaction Gibbs free energy, about -40 kJ mol^{-1}. These examples demonstrate that the solvation energy of a proton is an essential quantity for determining reliable computational values for the free energy of complexation by an acid.

Independent of the absolute values calculated, our results show that mono- and bidentate complexes at room temperature are energetically almost degenerate (Table 8) while bidentate complexes become more favourable with increasing temperature. The difference of the complexation Gibbs free energy between mono- and bidentate complexes increases (in absolute terms) from 1 kJ mol^{-1} to 5 kJ mol^{-1} when the temperature is raised from room temperature to 90 °C. This trend is independent of the model equation used, as these equations differ only by the representation of the solvated proton. These computational results suggest that the concentration ratio of bi- and monodentate complexes increases from about 2:1 at room temperature to 7:1 at 90 °C. As the bidentate conformer of uranyl monoacetate shows the stronger temperature effect and dominates at elevated temperatures, we ascribe the temperature dependence of uranyl acetate complexation to the bidentate coordinated species.

Neptunyl acetate complexation

Neptunyl(V) acetate has been choosen as an exemplary case for the detailed examination of a complexation reaction as the monoacetate complex is neutral. Thus, solvation effects are small and this facilitates the modeling. Table 9 lists the geometric parameters of neptunyl

Table 9. Geometry parameters[a] (in pm) of the five-coordinated Np(V) aquo ion and the monoacetate complex [NpO_2Ac] with mono-and bidentate coordination of the acetate ligand in comparison to experimental results.

		Np-O_t	Np-O_C	Np-C	Np-O_{eq}
NpO_2^+	calc.	183			254
	exp.	182-185			246-252
[NpO_2Ac]	calc. mono	184	249	347	253
	bi	184	252	290	253
	exp. pH = 0.6	183			251(4.5)
	2.7	184		291(0.7)	251(4.5)
	3.7	184		290(1.9)	251(5.2)

(a) Np-O_t – average neptunyl bond, Np-O_C – neptunium bond to carboxylate, Np-C – neptunium distance to carboxyl C, Np-O_{eq} – average equatorial neptunyl-ligand bond.

aqua and monoactate complexes. Coordination number 5 was assumed in these models as is typical for neptunyl(V) complexes [29,173-175].The neptunyl bond length Np-O_t of 183 pm as well as the average bond length of aqua ligands Np-O_{eq}, 254 pm, agree with available experimental data (Table 9). Acetate may coordinate to neptunyl in mono- or bidentate fashion. Employing a GGA functional, we calculated the bidentate five-coordinate complex to be ~15 kJ mol^{-1} more stable than the monodentate complex. As result of acetate coordination, the neptunyl bond increases by 1 pm (Table 9). Np-O_C bonds to the acetate ligand are only slightly shorter than bonds to aqua ligands. These bonds are 249 pm for monodentate and 252 pm for bidentate coordination, while the average bonds to aqua ligands are 254 pm in either case. From these results a value of 253 pm for Np-O_{eq} is calculated, independent of the coordination mode (Table 9). These results are in rather good agreement with a recent EXAFS study of neptunyl acetate complexes in aqueous solution [176] by the project partner Helmholtz-Zentrum Dresden-Rossendorf. In that study Np-O_t was measured at 184 pm and Np-O_{eq} at 251 pm. Interestingly, both these quantities do not change with increasing pH. A measured Np-C distance of about 290 pm also agrees very well with our calculations (Table 9), confirming a bidentate coordination of the acetate ligand. These experimental results support our more general result that average equatorial actinyl-oxygen distances, here Np-O_{eq}, depend mainly on the coordination number, but not on the type or number of ligands (Table 9).

In addition to optimizing stable structures we traced the reaction of solvated neptunyl(V) with an acetate ligand starting from a five-coordinate outer-sphere complex, employing a restricted geometry optimization (Fig. 5). We used the decreasing distance Np-C as a reaction coordinate. For the outer-sphere complex a Np-C distance of 498 pm was calculated. With decreasing Np-C distance, at about 400 pm, a barrier is reached on the way to monodentate coordination of the ligand. In the course of that reaction an aqua ligand is

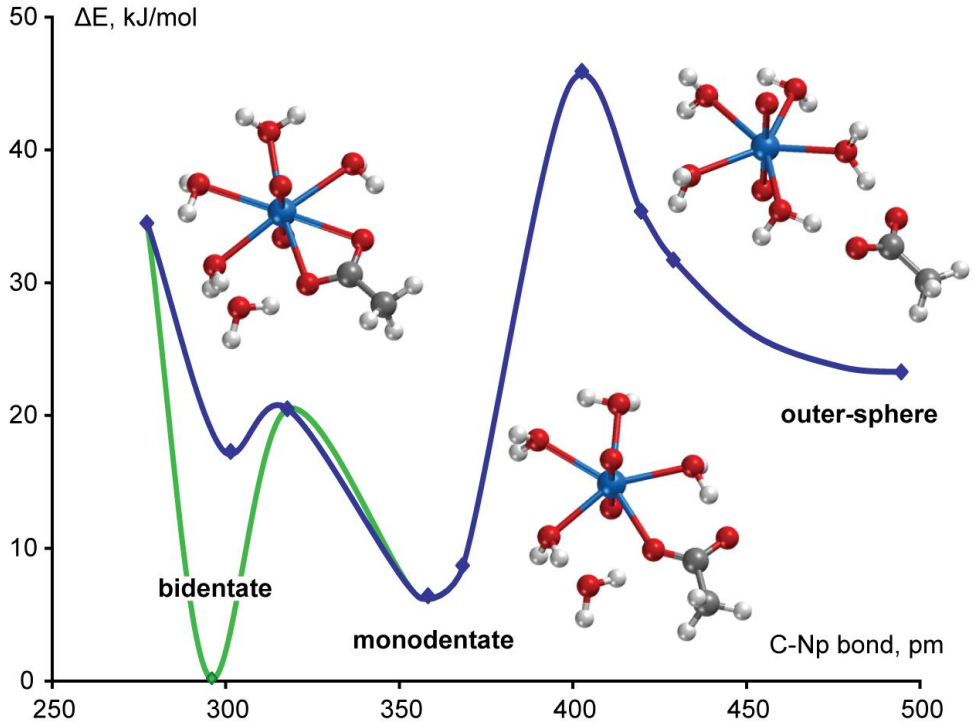

Figure 5. Complexation of neptunyl(V) by acetate. Reaction pathway from outer-sphere to inner-sphere mono- and bidentate complexes as a function of the distance Np-C. For bidentate complexation, six- (blue) and five-coordinate species (green) were optimized.

expelled from the first solvation shell, leading to a five-coordinate monodentate species. Further decrease of Np-C results in bidentate coordination of the acetate ligand, at Np-C = 298 pm, with the overall coordination number 6 of neptunyl. This species is energetically by ~10 kJ mol^{-1} less stable than the monodentate complex (Fig. 5). Removal of a second aqua ligand from the first coordination shell leads to a five-coordinate bidentate species, which is slightly more stable than the monodentate complex. From these results one may tentatively conclude that mono- and bidentate neptunyl monoacetate complexes are in a fast dynamic equilibrium while the outer-sphere complex, higher in energy by about 25 kJ mol^{-1}, is separated by a higher barrier of about 40 kJ mol^{-1}. Thus, although not noticed in the EXAFS results (Table 9) [176], monodentate complexes should contribute to the speciation of neptunyl(V) at low pH.

4.1.4 An(IV) complexes

Aqua ions and monohydroxides of uranium and neptunium in the oxidation state IV have been studied at the GGA level of DFT in aqueous solution as exemplary complexes of this less well explored oxidation state. The large charge of the complexes poses an additional challenge in computational studies because long-range solvation effects are important (see Section 4.3). Previous computational studies addressed uranium and neptunium(IV) aqua complexes, but there structure optimizations were limited to systems in the gas phase and by

Table 10. Calculated structure parameters[a] (GGA, distances in pm) of U(IV) and Np(IV) aqua complexes and monohydroxides as well as reaction energies (in kJ mol^{-1}) of adding an aqua ligand for coordination numbers CN = 8–10. All models for systems in aqueous solution.

CN	8	9	10	8	9
	An-O_W			ΔE	
U^{4+}	239	242	247	-64	-25
$[UOH]^{3+}$	247	250	255	-38	-17
Δ	8	8	8		
Np^{4+}	238	241	246	-36	-25
$[NpOH]^{3+}$	245	248	253	-33	-23
Δ	7	7	7		
	An-O_H				
$[UOH]^{3+}$	204	206	207		
$[NpOH]^{3+}$	205	205	208		

(a) CN – coordination number of actinide ion, An-O_W – average actinide bond to aqua ligands, An-O_H – bond between actinide ion and OH ligand.

symmetry constraints [177]. To the best of our knowledge, our calculations on the monohydroxides were the first such studies.

The aqua ions of An(IV) were modeled for coordination number CN = 8–10. With increasing CN, the average An-O distance was calculated to increase (Table 10), from 239 pm for CN = 8 to 247 pm for CN = 10 for U^{4+}. For neptunium, these bond lengths are by 1 pm shorter, in line with the smaller radius of the Np^{4+} ion. These results compare fairly well to EXAFS measurements of these quantities, 240–244 pm for uranium [178-182] and 237-240 pm for neptunium [29,174,183]. Thus, the tentatively best agreement with experiment is achieved for CN = 9 for uranium and CN = 8 for neptunium. The experimental studies suggest CN = 9–11 for uranium [178-182] as well as for neptunium [29,174,183]. Also our calculated energies of water addition to $[An(H_2O)_n]^{4+}$ favor complexes with higher coordination. Addition of an aqua ligand was calculated endothermic, by 64 kJ mol^{-1} for uranium and 36 kJ mol^{-1} for neptunium, for CN = 8. For CN = 9 this reaction energy decreases for both complexes to 25 kJ mol^{-1}. Taking into account that entropy corrections will favor lower coordination numbers as an additional aqua ligand is brought to the first coordination sphere, CN = 9 seems plausible for both aqua ions. For neptunium, CN = 8 in addition might be present as a minority species (Table 10). Longer An-O bonds were calculated with the hybrid B3LYP functional for complexes in the gas phase, ranging from 245 pm for CN = 8 to 255 pm for CN = 10 for uranium and being again slightly shorter for neptunium [177]. The typical contraction of bonds to aqua ligands due to long-range

Table 11. Calculated structure parameters (GGA, distances in pm) and Gibbs free energies (in kJ mol^{-1}) of addition of an aqua ligand of the Am(III) aqua ion for coordination 7–10.

	Am-O		ΔG
CN	VWN	BP	BP[a]
7	236		4
8	239	247	22
9	243	249	30
10	248		
Exp.[b]	247-249		

(a) BP single point at VWN geometries (b) Refs. [184-186].

solvation effects will bring these results in close agreement to ours. In that study results on energies were shown to favor CN = 9 for uranium and CN = 8–9 for neptunium [177].

Hydrolysis of an aqua ligand to yield the monohydroxide $[AnOH(H_2O)_n]^{3+}$ leads to an elongation of the bonds to aqua ligands, by 8 pm for uranium and 7 pm for neptunium, irrespective of the coordination number (Table 10). This finding, together with the observation that during the structure optimizaton none of the aqua ligands moved to a position in the second solvation shell, shows that up to CN = 10 steric repulsion is of minor importance for the structure of these complexes. For larger numbers of hydroxide ligands a corresponding lowering of coordination number due to increasing bonding competition between weakly bound aqua ligands and strong bound hydroxide ligands was demonstrated for Th(IV) in a quantum chemical study [99]. An-O_H bonds of the monohydroxide were calculated between 204 and 208 pm for CN = 8–10, showing a slight increase with increasing coordination number (Table 10). Interestingly, the tendency to slightly longer bonds for uranium compared to neptunium is broken for CN = 8 (Table 10). Energies of adding an aqua ligand are always lower for the monohydroxides compared to the aqua complexes of the same coordination number. This finding can be rationalized by bond competition between the hydroxide and the aqua ligands and the stronger metal-ligand bond of the latter. The exothermic reaction energies of adding an aqua ligand, 38 kJ mol^{-1} for CN = 8 and 17 kJ mol^{-1} for CN = 9 for uranium, 33 kJ mol^{-1} for CN = 8 and 23 kJ mol^{-1} for CN = 9 for neptunium, again suggest CN = 9 to be preferred when entropy effects are considered. More detailed thermodynamic calculations are in progress.

In summary, our calculations support CN = 9 for the aqua ion and the monohydroxide of U(IV) and Np(IV), based on geometry parameters in comparison to experimental findings as well energy considerations. Early hydrolysis of U(IV) and Np(IV) is geometrically characterized by the appearance of a short An-O bond of ~205 pm to the hydroxide ligand and an increase of the distance to the first hydration shell, by 7–8 pm.

Table 12. Calculated structure parameters (LDA, distances in pm) and Gibbs free energies (single point BP, Eq. (7), in kJ mol^{-1}) of complexation of Am(III) monoacetate with coordination numbers of the Am(III) ion of 7-10.

	mono				bi			
CN	Am-O_C	Am-O	Am-C	ΔG	Am-O_C	Am-O	Am-C	ΔG
7	238	239	341	55	238	240	277	51
8	241	242	340	62	241	243	279	52
9	243	245	334	66	243	245	282	49
10	244	249	343	68	245	249	283	55

(a) Am-O_C – americium bond to carboxylate, Am-O – average americium bond to all ligands, Am-C – americium distance to carboxyl C.

4.1.5 Am(III) complexes

Am(III) aqua ion

As a prerequisite for the examination of Am(III) complexes we modeled the aqua ion. EXAFS experiments gave an average Am-O distance of ~248 pm [184-186] and coordination numbers of 10±0.3 [184], 8.4±1 [185], and 7.4±1[186]. Our calculated results (Table 11) yield the energy of adding an aqua ligand at only 4 kJ mol^{-1} for coordination 7; the values for coordination numbers 8 and 9 are somewhat higher, 22 and 30 kJ mol^{-1}, respectively. Thus, coordination 7 and 8 are essentially degenerate, in agreement with the suggestion of a coordination of about 8 by more recent EXAFS results [185, 186]. While for lower coordination numbers VWN optimizations lead to shorter Am-O distances of 236-243 pm, BP results of 247 pm for CN = 8 and 249 pm for CN = 9 agree very well with experiment [184-186].

Am(III) acetate

Am(III) complexation with organic ligands was studied in detail for the standard model ligand acetate. Mono- and bidentate coordination of acetate were examined, varying the coordination number of Am^{3+} from 7 to 10. For all these complexes, as earlier for the aqua ion, we obtained the expected septet electronic configuration in our scalar-relativistic calculations. Table 12 collects the geometric characteristics of these complexes. As expected, the bond lengths Am-O_C from Am to the acetate ligand increase with increasing coordination number CN, from 238 pm for CN = 7 to about 245 pm for CN = 10, reflecting the increasing bond competition with aqua ligands. This competing effect also shows up in the average Am-O bond to all ligands, which increases from about 240 pm to 250 pm when CN is raised from 7 to 10. As for other carboxylate complexes (see above) [56,143,148], Am-O is independent of the coordination mode and thus may be used as fingerprint of the coordination number in EXAFS measurements. The coordination mode is best identified by the Am-C distance, about 340 pm for monodentate and 280 pm for bidentate complexes (Table 12). To inspect the stability of the complexes, the complexation reaction was

characterized by the Gibbs free energy of complexation with acetic acid (Table 12), which is directly relevant at low pH:

$$[Am(H_2O)_n]^{3+} + AcH \rightarrow [Am(H_2O)_{n-m}Ac]^{2+} + [H_3O]^{+} + (m-1)\ H_2O \qquad (7)$$

Here n is the coordination number, 7–10, and m = 1 for monodentate and 2 for bidentate acetate coordination. As shown by the endothermic Gibbs free energies, for all coordination numbers bidentate coordination is preferred. This preference ranges from 4 kJ mol^{-1} to 17 kJ mol^{-1}. The complexation Gibbs free energies, 50–55 kJ mol^{-1}, for bidentate complexes of various coordination numbers overestimate the experimental results of about 15 kJ mol^{-1}, derived from measured log β values of the project partner TU Dresden as well as earlier experiments [187]. The calculated Gibbs free energy of adding an aqua ligand to the complex with CN = 7 is 5 kJ mol^{-1} for the bidentate and 12 kJ mol^{-1} for the monodentate complex. Thus, species with CN = 7 and 8 are energetically nearly degenerate. Addition of a further aqua ligand to reach CN = 9 requires about 20 kJ mol^{-1}; thus a higher coordination is not favorable.

4.2 Adsorption of actinides on clay minerals

Adsorption on the surfaces of clay minerals is an important retardation mechanism, governing the distribution of actinides in the environment. A detailed understanding of this process is of timely interest for the risk assessment of possible deep geological repositories [188,189]. Despite a large amount of experimental studies on the adsorption of actinides at clay minerals [190-199], there are still many open questions, e.g., (*i*) what is the nature of the adsorbed species; (*ii*) which surfaces, basal or edge, are more preferred for adsorption; (*iii*) what are the main adsorption sites, etc. Computational approaches as applied in this project provide insight into these topics on the atomic level, hence are able to complement experimental investigations.

4.2.1 Clay mineral surfaces and surface models

Clay minerals are hydrous aluminum phyllosilicates, built of interconnected sheets of Si tetrahedra and Al octahedra to form layered structures. We studied 1:1 and 2:1 clay minerals. The 1:1 clay mineral kaolinite consists of one tetrahedral Si sheet bound to an octahedral Al sheet [200]. 2:1 clay minerals consist of an octahedral sheet sandwiched between two tetrahedral sheets. The simplest 2:1 clay mineral without substitutions is pyrophyllite [201]. Families of other clay minerals can formally be derived from these two prototypes by substitutions, which create permanently charged layers that are neutralized by interlayer counterions. As example, we modeled beidellite which exhibits substitutions of Si^{4+} by Al^{3+} in the tetrahedral sheet.

In general, clay minerals feature an ideal (001) cleavage plane, the so-called basal plane. The (001) surface of kaolinite can be terminated by Al octahedra – Al(o), or Si tetrahedra – Si(t), see Fig. 6. The (001) planes of 2:1 phyllosilicates are siloxane surfaces,

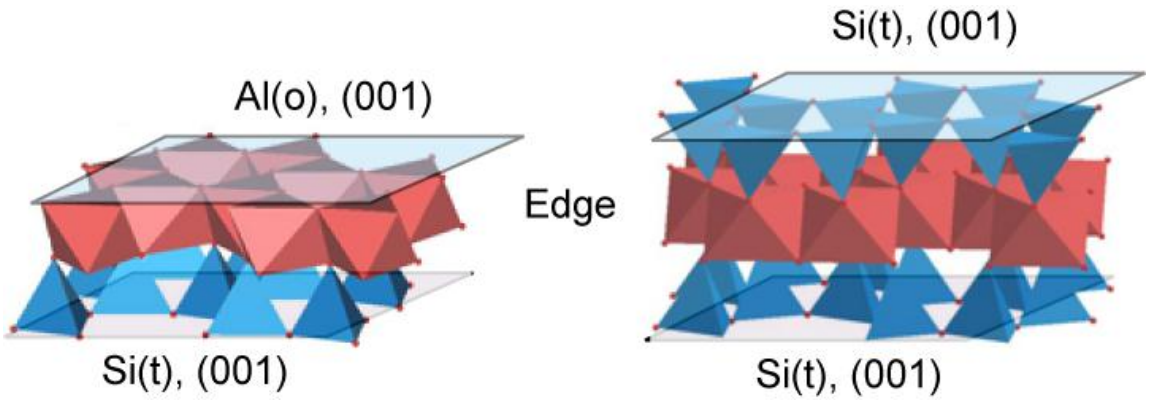

Figure 6. Structures of basal and edge surfaces of kaolinite and pyrophyllite.

formed by Si(t) planes. We modeled the surfaces of clay minerals by invoking the periodic supercell approach. Potential artifacts due to translational symmetry are avoided by rather large unit cells that contain up to a few hundreds of atoms.

To study adsorption on the basal surfaces of kaolinite we used (2×1) and (2×2) unit cells that comprised only a single two-sheet layer [105]. Adsorption of uranyl on bare surfaces was modeled using both the local density approximation (LDA) and the generalized gradient approximation (GGA). To account for surface solvation 20 water molecules, covering a (2×2) unit cell (surface area: 1.82 nm^2) of the (001) kaolinite surface by about a monolayer, were introduced into the quantum chemical model. As LDA is known to overestimate weak interactions, all models with surface solvation were optimized at the GGA level to improve the description of hydrogen bonds.

Fig. 7a shows an optimized kaolinite one-layer model. Two thirds of the OH groups, "uOH", on the optimized (001) Al(o) kaolinite surface are in "upright" orientation, perpendicular to the (001) plane. The remaining OH groups, "lOH", are oriented parallel to the (001) plane [105]. Fig. 7b presents a top view of the Al(o) (001) surface of kaolinite, featuring both uOH and lOH moieties. The Si(t) surface is rather rigid; it hardly undergoes any relaxation compared to the bulk structure. Surface solvation of the Al(o) (001) surface of kaolinite did not change the ratio between upright and lying OH groups. The hydroxide groups formed hydrogen bonds with water molecules, of types $uOH\cdots OH_2$ and $lHO\cdots H_2O$. These H bonds stabilized both types of surface OH groups. The Si(t) (001) surface of kaolinite was shown to be hydrophobic as the 20 water molecules tend to form a water cluster far above the surface, forming only two H bonds with surface oxygen centers [202].

The basal (001) surface of charged 2:1 clay minerals of beidellitic type was modeled by a (2×2) unit cell (area: 1.82 nm^2) that contained two structural substitutions of Si^{4+} centers by Al^{3+} cations. The charge was neutralized by two Na^+ counterions, each solvated by five water molecules, and adsorbed as outer-sphere complexes on the siloxane surface. Surface solvation in this case was represented by 16 additional water molecules.

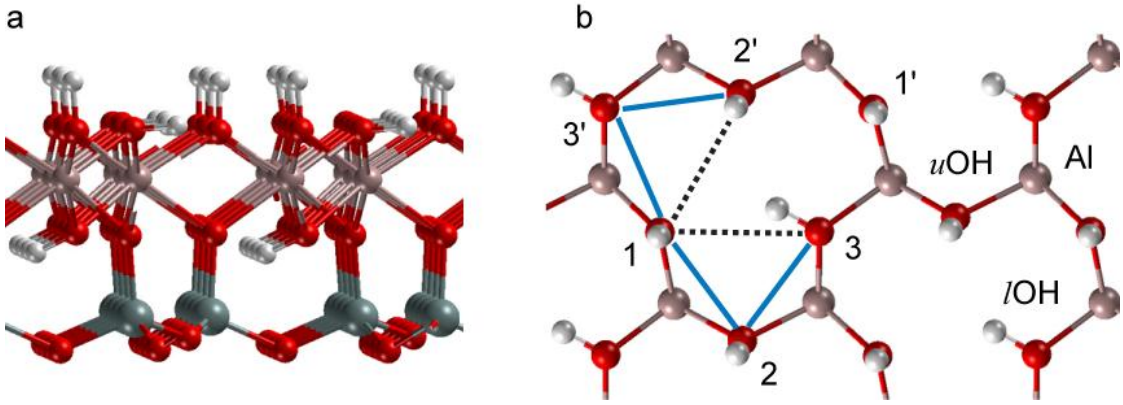

Figure 7. (a) Side view of a single-layer model of kaolinite where atomic "sublayers" are indicated. (b) Top view of the Al(o) basal (001) surface of kaolinite. uOH – upright surface OH group, lOH – lying surface OH group. Symmetry inequivalent surface oxygen centers are numbered for convenience. Corresponding equivalent centers are labeled by a prime. Solid blue lines – short-bridge sites, dashed lines – long-bridge sites.

Besides basal planes, clay mineral particles exhibit edge surfaces (Fig. 6) which are assumed to be more reactive [203]. They are terminated by unsaturated oxygen centers which can exchange protons with the solution and in this way generate a pH-dependent surface charge. The exact atomic structures of edge surfaces are not known. Various empirical models exist to predict favorable edge planes and their atomic structures. The most popular among them is the crystal growth theory of Hartmann and Perdok [204-206]. For dioctahedral 2:1 clay minerals it predicts six edge surfaces: (010), (100), (±110), and (±130).

For the kaolinite, we studied the (010) surface as an exemplary edge surface [107]. The terminations of edge surfaces can be constructed by (formally) cutting the crystal parallel to the surface of interest, breaking the weakest bonds, and preserving the stoichiometry of Si and Al ions. Using this strategy, we identified four possible terminations for the (010) kaolinite surface. Two of these terminations, S0 and S1, were selected for further studies as more favorable based on an empirical bond strength model [207] and considerations regarding the dissolution of kaolinite [107]. Both terminations of the (010) kaolinite surface were modeled with (2×2) unit cells of ~1.5 nm^2 surface area. Although of different surface structure, they comprise similar surface groups, SiOH, AlOH, $AlOH_2$. The construction of the terminations and the protonation schemes have been discussed in detail [107]. Protons of silanol groups move to neighboring aluminol groups, forming SiO^- and two $AlOH_2$ groups [107]. Surface solvation was approximated by 22 adsorbed water molecules. Although smaller in area than the (001) surface of kaolinite, the (010) surface is rougher; therefore, more water molecules were used to cover it. The main effect of solvation of the edge surfaces is a rearrangement of protons on the surface [107].

Pyrophyllite is the only mineral for which the atomic structures of different edge

terminations have been computationally characterized at the atomic scale [208,209]. We chose the (010) and (110) edge surfaces of pyrophyllite for examining uranyl adsorption [210]. Pyrophyllite edge surfaces models were modeled with (2×1) unit cells of ~1.1 nm^2 surface area, covered by 15 water molecules to approximate solvation. In contrast to kaolinite, solvation does not lead to rearrangement of protons. Thus, bare and solvated edge surfaces of pyrophyllite exhibit the same surface groups. Compared to kaolinite, edge surfaces of pyrophyllite are more complex. Besides aluminol and silanol surface groups they also offer mixed sites AlOSi with oxygen centers bound to aluminum and silicon. In our studies of uranyl adsorption on edge surfaces of substituted pryophyllite, modeling the mineral beidellite, we applied a monoclinic unit cell which is common to various charged 2:1 clay minerals. As for pyrophyllite edge surfaces, a (2×1) unit cell and 15 water molecules to approximate surface solvation were used. The same types of surface groups are present as on edge surfaces of pyrophyllite.

Solvation of surfaces and complexes adsorbed on them was directly introduced into the quantum chemical models by explicit water molecules. As an approximation when calculating the energetics, we assumed that long-range solvation effects are comparable for the surfaces with and without adsorbates. For the molecular species appearing in formal adsorption reactions, like H_2O, H_3O^+, $[UO_2(H_2O)_5]^{2+}$ (see below), solvation energies including long-range effects were estimated using the COSMO solvation model as implemented in the program ParaGauss [65].

4.2.2 Adsorption on kaolinite

Three topics will be addressed in this section. First, results on uranyl adsorption on basal planes of kaolinite are described [105] together with surface solvation effects [106]. As the Si(t) basal surface of kaolinite was shown to be less reactive regarding uranyl adsorption [105] than the Al(o) surface, the following section on neptunyl NpO_2^+ adsorption contains only models of adsorption complexes on the hydroxylated Al(o) surface. Finally, computational results for uranyl adsorption on edge surfaces of kaolinite including surface solvation effects [107] are discussed.

Adsorption of uranyl(VI) on basal surfaces

The two principal types of species postulated for metal adsorption at mineral surfaces are inner-sphere and outer-sphere complexes. The adsorption of uranyl on the bare Al(o) and Si(t) (001) basal surfaces of kaolinite was studied in detail by comparing mono- and bidentate short- and long-bridge inner-sphere as well as outer-sphere complexes [106,105]. The short-bridge bidentate sites are formed by surface O centers bound to the same Al atom (Fig. 7b, solid lines), while the long-bridge sites are two O centers bound to different Al atoms (dashed lines). Uranyl was shown to adsorb at long-bridge sites only when both surface AlO groups of the site are deprotonated [106]. The uranyl complex adsorbed at a long-bridge AlO-AlOH site converged to a complex at the nearest short-bridge AlOOH site

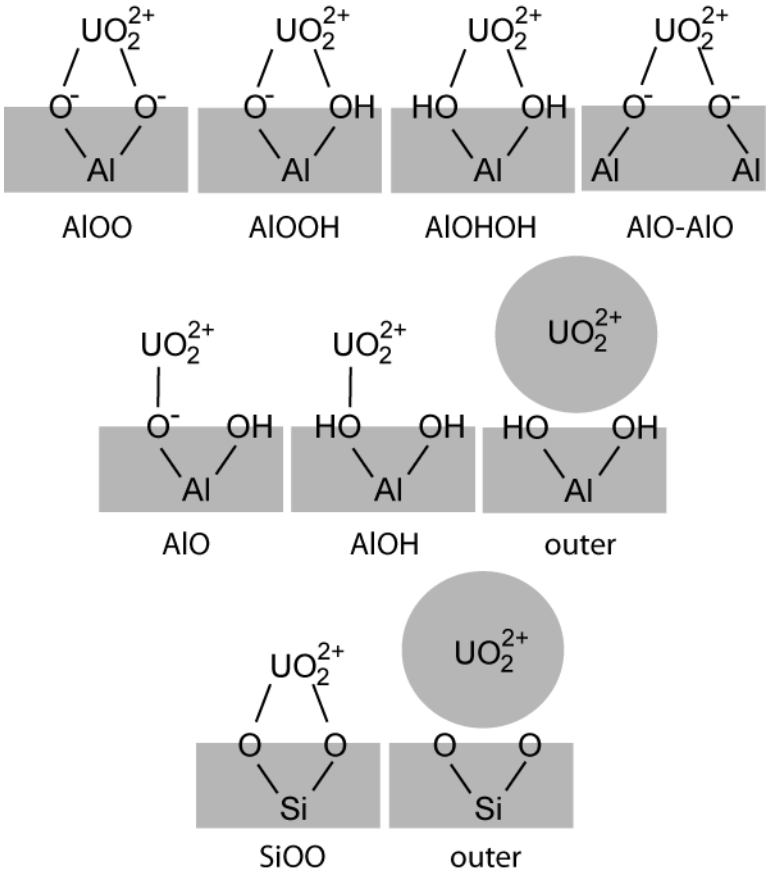

Figure 8. Schematic representation of the model adsorption complexes studied for the basal Al(o) and Si(t) surfaces of kaolinite: bidentate short-bridge (AlOO, AlOOH, AlOHOH, SiOO) and long-bridge (AlO-AlO) inner-sphere complexes, monodentate inner-sphere (AlO, AlOH) and outer-sphere complexes.

[106]. This result suggests that sites available for uranyl adsorption are pH dependent, as the long-bridge site is occupied only when deprotonated. Adsorption at different pairs of surface groups (uu, ul) was also examined [105,106], but turned out to be similar for chemically similar sites (AlOO, AlOOH, etc.).

Fig. 8 schematically presents all adsorption complexes modeled. The Al(o) surface implies more adsorption sites due to its hydroxylation and deprotonation of surface OH groups at higher pH. The Si(t) surface is commonly assumed to be less reactive as it exhibits only coordinatively saturated oxygen centers. The adsorption complexes shown in Fig. 8 imply charged unit cells. The program VASP provides accurate compensating corrections for charged unit cells only for cubic lattices. Therefore, models with the neutral unit cell had to be created by invoking surface defects. For modeling uranyl adsorption on a Si(t) surface, two protons were removed at the opposite side [Al(o)] of the slab model to compensate the charge of the adsorbed uranyl ion. When modeling uranyl adsorption at an Al(o) surface, two silanol defects per (2×2) unit cell were introduced at the opposite side [Si(t)] which may be deprotonated when necessary for charge compensation. For the details see Ref. 105.

Table 13. Calculated structural parameters[a] (in pm) of various models of adsorption complexes of uranyl on the bare basal Al(o) (001) surface of kaolinite. Experimental results are provided for comparison.

Site	U-O_t	U-O_{surf}	U-O_W	U-O_{eq}	U-Al
LDA					
AlOO	185	208/223	251/253/253	237	308
AlOOH	184	210/260	247/248/248	243	327
GGA					
AlOO	187	213/219	263/266/266	245	311
AlO-AlO	187	218/229/260	266/271	249	330/340
AlOOH	186	213/264	257/260/262	251	332
outer-sph		U-O_W			
Model 1	184	242/250/256/265/281		253	
Model 2	184	238/249/257/263/279		257	
Exp.					
Ref. 211	180	228(×2), 248(×3)		240	330
Ref. 212	180			236-240	310/330

(a) U-O_t – uranyl bond, U-O_{surf} – U bonds to the surface O, U-O_W – uranyl bonds to aqua ligands, U-O_{eq} – average equatorial uranyl-ligand bond, U-Al – distance to surface Al center.

Comparison of exemplary adsorption complexes on the bare Si(t) surface with the corresponding species at the Al(o) surface revealed that the Si(t) surface is energetically less favorable for uranyl adsorption, in agreement with common expectations [105]. Complexes with monodentate coordination of uranyl on the bare Al(o) surface were calculated to be of similar stability as the bidentate adsorption complexes [105]. The adsorption complex at the long bridge AlO-AlO site exhibits a third contact to a neighboring AlOH group [106]. However, as monodentate complexes feature longer U-Al contacts than bidentate complexes at sites of the same degree of deprotonation, comparison of U-Al distances with EXAFS results [197,211,212] suggests bidentate species to be present [105]. Among various bidentate inner-sphere complexes on the bare Al(o) surface of kaolinite those at deprotonated short-bridge sites of the types AlOO and AlOOH and at the long-bridge AlO-AlO sites agree reasonably well with EXAFS results (Table 13) with the exception of the too long uranyl bond. These complexes also exhibit the shortest values for U-Al distances (AlOO: 308 pm, AlOOH: 327 pm) and average distances U-O_{eq} of uranium to equatorially coordinated O atoms (AlOO: 237 pm, AlOOH: 243 pm) [105]. The results just mentioned were obtained at the LDA level. When comparing calculated GGA results to experiment, one should take into account that GGA functionals tend to overestimate geometric parameters [106]. At the GGA level, the following results were obtained: U-Al at AlOO – 311 pm, AlO-AlO – 330/340 pm, and AlOOH – 332 pm; U-O_{eq} at AlOO – 245 pm, AlO-AlO – 249 pm, AlOOH – 251 pm (Table 13). Suitably adjusted calculated results (for details

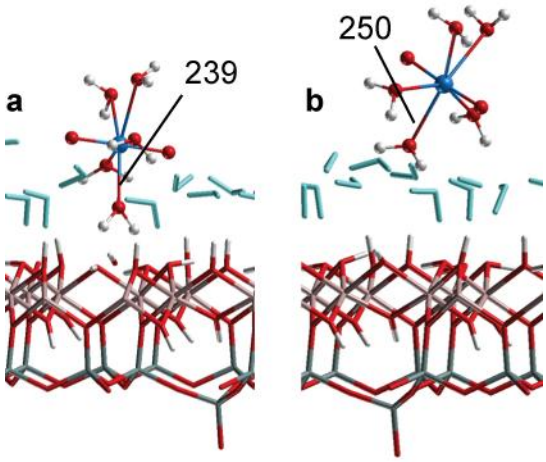

Figure 9. Outer-sphere adsorption complexes of uranyl at the (001) Al(o) surface of kaolinite including surface solvation: (a) uranyl in contact with the surface via an aqua ligand of the first solvation shell; (b) first solvation shell of uranyl not in contact with the surface.

see Refs. 106 and 107) are in line with experimental results obtained for pH values close to the pH of neutral charge of kaolinite (pH_{ZPC} = 5.5) and above where deprotonated sites are to be expected. In addition, deprotonation of surface hydroxide groups will be facilitated in the field of adsorbed uranyl cations. Thus, adsorption at deprotonated sites is also possible for pH below pH_{ZPC}.

Surface solvation modeled by a monolayer coverage of water molecules only slightly affects inner-sphere bidentate adsorption complexes. Compared to the adsorption complexes on the bare Al(o) surface, U-Al distances were elongated by 3–4 pm; the average equatorial U-O_{eq} distances decreased by 2 pm on average and uranyl U-O_t bonds were only slightly elongated, by 1–2 pm [106]. Thus, surface solvation does not seem to play a decisive role for a qualitatively correct modeling of uranyl adsorption on basal crystal planes of kaolinite.

Although outer-sphere adsorption on the bare Al(o) kaolinite surface was not found to be preferred, some interesting trends were observed which can be extended to other clay minerals. A model of an outer-sphere complex has been set up where the solvated uranyl ion is in direct contact with the support via one of the aqua ligands of its first coordination sphere. This model exhibits one shorter U-O_W distance, 242 pm (at the GGA level), to an aqua ligand adjacent to the surface; see Model 1 in Table 13. The other U-O_W bonds are in the range of 250–280 pm [43]. One of these aqua ligands is attracted by the surface, resulting in a rather long U-O_W contact of 280 pm. Therefore, we also explored the effect of an additional water molecule at that location on the surface (Model 2 in Table 13). Yet, a very similar outer-sphere complex with one short U-O_W contact to the aqua ligand directed to the surface and one rather long U-O_W bond (279 pm) was obtained. Thus, outer-sphere complexes at the bare Al(o) surface exhibit a "splitting" of the first coordination shell. This finding is at variance with the common expectation based on experimental findings that

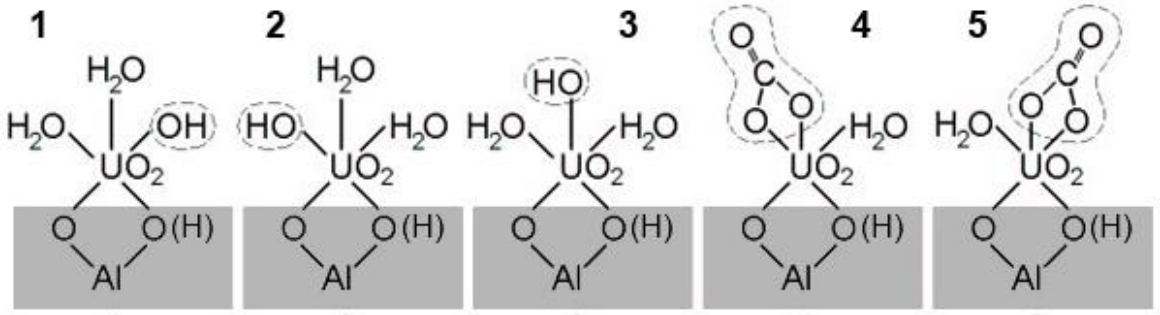

Figure 10. Schematic representation of adsorption complexes of $[UO_2OH]^+$ and $[UO_2CO_3]^0$ on the basal Al(o) (001) surface of kaolinite.

outer-sphere complexes should show structural characteristics (very) similar to those of a solvated uranyl ion [195]. Similar results also hold at the Si(t) surface.

From these results one can conclude that experimentally detected adsorbed species of solvated uranyl, classified as outer-sphere complexes, should involve more than a single layer of water molecules between uranyl and the surface. To check this, two types of outer-sphere models of uranyl adsorbed at the solvated Al(o) surface were studied [43]. The first model of the outer-sphere complex exhibits a direct contact of the first solvation shell with the surface (Fig. 9a). The second model deposits the solvated uranyl ion above the monolayer of adsorbed water (Fig. 9b). The first model includes explicit solvation but it shows qualitatively the same structural parameters as the outer-sphere complex without surface solvation, namely a split first coordination shell of uranyl with a shorter contact to the water facing the surface (see Fig. 9a). Geometry parameters of the optimized second model do not show any appreciable splitting of the U-O_W bond lengths: all five U-O_W bonds are in the range of 250–265 pm [43]. These model calculations confirm the assumption that more than one water layer should be present between an adsorbed uranyl ion and the surface to reproduce the experimentally suggested structural characteristics of outer-sphere species.

Adsorption of complexes on the basal Al(o) (001) surface of kaolinite

Apart from the solvated uranyl ion, other uranyl species like hydroxide and carbonate complexes are present in solution at environmental conditions. The most common mononuclear uranyl compounds at acidic to neutral pH are uranyl monohydroxide, $[UO_2OH]^+$, and the uranyl-carbonato complex, $[UO_2CO_3]^0$ [120]. We studied the adsorption of these species on the AlOO and AlOOH sites of the bare Al(o) basal (001) surface of kaolinite. These sites are charged, -2 *e* and -1 *e*, while the adsorbates are either neutral or positively charged, +1 *e*. To achieve an overall neutral unit cell a proton was attached to one of the O atoms on the opposite Si(o) side of the slab models. The correction for such a neutralization was estimated as deprotonation energy of the cluster $[Si(OH)_3\text{-}OH\text{-}Si(OH)_3]^+$.

Various positions of the moieties OH^- and CO_3^{2-} on the surface were modeled. Fig. 10 shows schematically the adsorption complexes for both types of sites studied. All three

Table 14. Calculated structural parameters[a] (in pm) for the most stable adsorption complexes of UO_2OH^+ and UO_2CO_3 at the AlOO and AlOOH sites of the Al(o) (001) kaolinite surface. Data for adsorbed UO_2^{2+} on the corresponding sites are given for comparison.

Site	Adsorbate	Model[b]	U-O_t	U-O_{surf}	U-OH/O_C	U-O_W	U-O_{eq}	U-Al
AlOO	UO_2^{2+} [c]		187	213/219		265	245	311
	UO_2OH^+	1	187	221/230	224	267	242	315
	UO_2CO_3	5	187	234/235	225/240	263	240	319
AlOOH	UO_2^{2+} [c]		186	213/264		260	251	332
	UO_2OH^+	1’	185	218/270	220	258	245	338
	UO_2CO_3	5’	186	228/268	223/239	255	243	338

(a) U-O_t – uranyl bond, U-O_{surf} – U bonds to the surface O, U-O_W – uranyl bonds to aqua ligands, U-O_{eq} – average equatorial uranyl-ligand bond, U-Al – distance to surface Al center. (b) For the designations of the models see Fig. 10. (c) Ref. 106.

adsorption complexes of $[UO_2OH]^+$ at the AlOO site (models 1, 2, and 3) are very close in energy. Model 1 is the most favorable; model 2 is only 3 kJ mol^{-1} and model 3 by 9 kJ mol^{-1} less stable. For adsorption of $[UO_2OH]^+$ on the singly deprotonated AlOOH site, models 1 and 3 are energetically degenerate, while model 2 is 33 kJ mol^{-1} less stable. This is tentatively rationalized by the position of the OH ligand close to the O^- center of the AlOOH adsorption site in model 2 which might cause repulsion. For $[UO_2CO_3]^0$, adsorbed at both AlOO and AlOOH sites, model 5 is 7–9 kJ mol^{-1} more favorable than model 4.

Structural parameters of the most favorable adsorption complexes at each site are collected in Table 14. Data for the uranyl ion adsorbed on the corresponding sites are given for comparison. First of all, note that the terminal U-O_t bonds are very similar for all adsorbates at a given adsorption site. U-O_t for the uranyl complexes adsorbed on the AlOO site is 187 pm, while on the AlOOH site it is slightly shorter (185–186 pm) due to weaker interaction with the partially protonated site. Due to the lower charge of the $[UO_2OH]^+$ adsorbate the bonds to the surface are weaker compared to UO_2^{2+} and consequently longer by ~10 pm (Table 14). As a result the U-Al distance increases slightly too, from 311 to 315 pm at the AlOO site and from 332 to 338 at the AlOOH site. Due to bond competition the U-OH bond for the adsorbed uranyl monohydroxide, 220–224 pm, is longer than for the solvated $[UO_2OH]^+$ species (214 pm, see also Section 4.1.1). Also, the average U-O_{eq} value for adsorbed $[UO_2OH]^+$ is slightly shorter, by 3–6 pm, than for UO_2^{2+}.

The neutral adsorbate $[UO_2CO_3]^0$ exhibits bonds to the surface of 234–235 pm for the AlOO site and 228–268 pm for the AlOOH site. In general, the U-O_{surf} bonds elongate with the decreasing charge of the adsorbate: UO_2^{2+}, $[UO_2OH]^+$, $[UO_2CO_3]^0$. The U-Al distances follow the same trend. Interestingly, the average value U-O_{eq} shortens to 240 and 243 pm for the $[UO_2CO_3]^0$ complex adsorbed on the AlOO and AlOOH sites, respectively. Thus, with decreasing charge of the adsorbate, the U-O_{eq} values shorten slightly: 245 pm for

UO_2^{2+}, 242 pm for $[UO_2OH]^+$, and 240 pm for $[UO_2CO_3]^0$ adsorbed at the AlOO site. For the AlOOH site, the corresponding values are 251, 245, and 243 pm.

In general, adsorption complexes on singly deprotonated AlOOH sites are quasi monodentate species (Table 14). They all exhibit one rather short contact to the surface, 213–228 pm, and one rather long U-O_{surf} bond of 264–270 pm. Bonds to the neutral AlOH surface groups are the longer ones of these distances; these values are even slightly longer than the average U-O_W distances to the aqua ligands (Table 14).

Adsorption of neptunyl(V) on basal surfaces

The adsorption of neptunyl NpO_2^+ on the basal surface of kaolinite was exmained in similar manner as uranyl. In view of the reduced charge of the complex, a weaker interaction with the surface was expected. The study focused on the basal Al(o) (001) surface, considering bidentate, monodentate, and outer-sphere adsorption complexes (Fig. 11). All complexes were modeled in a (2×1) surface unit cell to save computational effort. Experimentally, the coordination number of neptunyl is known to vary from 4 to 5 [29,213]. We modeled both four- and five-coordinated NpO_2^+. The corresponding adsorption energies were calculated with reference to $NpO_2(H_2O)_4^+$ and $NpO_2(H_2O)_5^+$, respectively. Thus, the change of coordination number of neptunyl is not included in the estimated energies.

The structure parameters of the adsorption complexes on singly deprotonated adsorption sites of Al(o) kaolinite are collected in Table 15. The corresponding adsorption energies, also presented in Table 15, are estimated according to the formal equation

$$\text{Surf-H} + NpO_2(H_2O)_n^+ \rightarrow \text{Surf-}NpO_2(H_2O)_{n-m-1} + m\ H_2O + H_3O^+ \quad . \qquad (8)$$

In Eq. (8) the coordination number n of the neptunyl ion, n = 4 or 5, implies m = 1 for bidentate adsorption and m = 0 for monodentate adsorption. Several adsorption complexes were explored for certain types of sites, reflecting not equivalent surface O centers for the adsorption. Results for inner-sphere adsorption of five-coordinated neptunyl on singly deprotonated sites suggest that mono- and bidentate complexes may coexist. Energetically they differ by 20 kJ mol^{-1} only, in favor of bidentate coordination. All bidentate adsorption complexes on AlOOH adsorption sites exhibit similar geometry parameters and adsorption energies. The structure parameters of the monodentate five-coordinated neptunyl complex at the AlO site are very similar to those for bidentate complexes on AlOOH sites, except for the Np-Al distance. For monodentate coordination, the Np-Al distance is considerably longer. Similar results were determined for the adsorption complexes with CN = 4. Furthermore, the estimated adsorption energies of four- and five-coordinated neptunyl are very close. The only differentiating characteristic of the adsorption complexes with CN = 4 and CN = 5 is the average equatorial distance Np-O_{eq}, ~250 pm and ~258 pm, respectively (Table 15).

Table 15. Calculated structural parameters (in pm) and adsorption energies (in kJ mol^{-1}) of adsorption complexes of neptunyl on the Al(o) basal (001) surface of kaolinite. Data are given for singly deprotonated (q = -1 *e*) and neutral sites (q = 0 *e*). For the designations of the sites, see Fig. 11.

Site, q = -1	Np-O_t	Np-O_{surf}	Np-O_W	Np-O_{eq}	Np-Al	ΔE
CN = 5						
$[NpO_2(H_2O)_5]^+$	181			257		
AlOOH	187	220/279	249/269/275	258	335	125
	186	219/274	259/265/267	257	334	145
AlO	185	229	258/258/270/273	258	373	144
CN = 4						
$[NpO_2(H_2O)_4]^+$	180			250		
AlOOH	186	220/272	247/259	250	335	129
	185	224/275	248/257	251	334	150
AlO	185	225	248/255/258	248	373	128
Site, q = 0						
CN = 5						
AlOHOH	186	263/267	257/262/263	262	361	-119
	187	247/275	257/259/264	260	362	-119
outer	183		259/261/262/ 265/275	264		-104
CN = 4						
AlOHOH	186	254/259	254/254	255	355	-76
outer	184		246/248/259/259	253		-160
Exp.[b]						
pH 8-10	185-187			245-250		

(a) Np-O_t – neptunyl bond, Np-O_{surf} – Np bonds to the surface O, Np-O_W – neptunyl bonds to aqua ligands, Np-O_{eq} – average equatorial neptunyl-ligand bond, Np-Al – distance to surface Al center. (b) Coordination number of terminal O fixed at 2, coordination number of equatorial O fixed at 4. Ref. 214.

Table 15 also collects structural data and adsorption energies for neptunyl inner-sphere adsorption at neutral AlOHOH sites as well as outer-sphere complexes. The adsorption energies on the neutral surface were estimated according to

$$\text{Surf} + NpO_2(H_2O)_n^+ \rightarrow \text{Surf-}NpO_2(H_2O)_{n-m} + m\ H_2O \qquad (9)$$

In Eq. (9) the coordination numbers n of the neptunyl ion, n = 4 or 5, result in m = 2 for bidentate adsorption and m = 0 for the outer-sphere complexes. Bidentate adsorption of neptunyl on neutral sites AlOHOH shows a clear preference for coordination number 5. In general, adsorption complexes of NpO_2^+ on neutral sites of the Al(o) kaolinite surface are characterized by longer bonds to surface AlOH groups, and, in consequence, longer Np-Al and Np-O_{eq} distances compared to deprotonated sites. Unfortunately, inherent limitations of

the model prevent a comparison of adsorption energies at sites of different charge. A detailed discussion can be found in Refs. 105 and 106.

In contrast to uranyl on kaolinite, the solvated neptunyl ion adsorbed as outer-sphere complex does not exhibit any "splitting" of the Np-O bonds in the first coordination shell. The Np-O bonds vary from 259 to 275 pm for CN = 5 and from 246 to 259 pm for CN = 4 without any clear separation into two groups. Energetically, outer-sphere complexes with CN = 4 are significantly more favorable than complexes with CN = 5. Outer-sphere complexes were also calculated to be energetically more favorable than inner-sphere bidentate complexes at neutral AlOHOH sites.

Table 15 also provides EXAFS results of the project partner Universität Mainz for the adsorption of neptunyl on kaolinite [214]. These data were determined for neptunyl adsorption on kaolinite in Ar atmosphere at pH 8, 9, and 10. Coordination numbers for the resolved Np-O bonds were fixed to 2 and 4 for terminal and equatorial oxygen atoms, respectively [214]. The experimentally resolved Np-O_t bonds 185–187 pm, agree very well with the results calculated for the inner-sphere adsorption complexes. The EXAFS values of Np-O_{eq} vary from 245 to 250 pm, again agreeing very well with results calculated for inner-sphere adsorption complexes with CN = 4. The optimized results for adsorption complexes with CN = 5 exhibit ~10 pm longer Np-O_{eq} distances, compared to experiment. The Np-Al/Si shell was not modeled in this EXAFS analysis because of the low signal-to-noise level of the data [214]. Thus, comparison of our results with the experimental data shows the best agreement for the inner-sphere adsorption of four-coordinated neptunyl. However, such perfect agreement with experiment may be fortuitous as the present models do not include surface solvation. Recall also that structural parameters optimized with a GGA exchange-correlation functional likely are overestimated. Furthermore, the smaller (2×1) surface unit cell, compared to the (2×2) unit cell used when modeling uranyl adsorption, represents a larger surface coverage. To probe effects of the lower coverage on neptunyl adsorption, several adsorption complexes were also optimized using the larger (2×2) surface unit cell. Structure parameters hardly changed (less than 2 pm), compared to the analogous complexes modeled in the smaller unit cell. At lower coverage, the adsorption complexes in general were stabilized by ~5 kJ mol^{-1}. Thus, the size of the unit cell does not play a decisive role for the calculations presented in this study. Surface solvation shows only slight effects on inner-sphere bidentate adsorption, just as calculated for uranyl on the basal Al(o) kaolinite surface. Again, surface solvation can be omitted when striving for qualitatively correct models of actinyl adsorption complexes on basal crystal planes of kaolinite.

Adsorption of uranyl(VI) on edge surfaces

The two terminations of the (010) edge surface of kaolinite selected for adsorption studies exhibit two types of adsorption sites, (*i*) aluminol sites, AlOO, AlOOH, AlOHOH, and (*ii*) mixed sites where both aluminol and silanol surface groups are involved, AlO(H)-SiO(H).

Table 16. Calculated structural parameters[a] (in pm) of more stable adsorption complexes of uranyl on various solvated surfaces of kaolinite.

		$U\text{-}O_t$	$U\text{-}O_{surf}$	U-OH	$U\text{-}O_W$
Al(o) (001)	AlOO	187	220/222		247/253/271
	AlO-AlO	188	222/223/258		252/259
S0 (010)	AlOHOH	185	236/254	223/229	275
S1 (010)	AlOH-SiO-AlOH	185	244/245/219		239/256

(a) $U\text{-}O_t$ – uranyl bond, $U\text{-}O_{surf}$ – U bonds to the surface O, U-OH – uranyl bonds to OH ligands resulting from water deprotonation, $U\text{-}O_W$ – uranyl bonds to aqua ligands.

All these sites were examined for the adsorption of uranyl, first without addressing surface solvation. Only bidentate adsorption complexes were studied because monodentate complexes exhibit U-Al/Si distances that are significantly longer than those resolved in EXAFS experiments of uranyl adsorption on kaolinite [197,211,212].

During optimization most of these models of adsorption complexes changed chemically as aqua complexes of the adsorbed uranyl deprotonated [202], resulting in uranyl monohydroxide as adsorbate. A proton of the first coordination shell of uranyl moved to the surface. Various uranyl complexes adsorbed at sites of the same charge (q = -2 *e* or -1 *e*) were calculated close in energy. Most of the complexes modeled exhibit similar characteristic structure parameters, with $U\text{-}O_{eq}$ = 237–243 pm and U-Al = 316–333 pm (LDA results [202]). These calculated data are in a good agreement with available experimentally determined values of $U\text{-}O_{eq}$, 236–240(±4) pm [197]. Experimentally determined U-Al/Si distances of 310 pm and 330 pm were derived by fitting a broad peak of the EXAFS spectrum between ~300 pm and 335 pm [197]. As we did not find two U-Al distances in this range for any complex, one can expect a broad distribution of such distances which, in turn, may indicate a variety of adsorption complexes, coexisting at certain environmental conditions.

To explore surface solvation effects, uranyl adsorption complexes were modeled on both terminations of the solvated (010) edge surface of kaolinite [107]. In addition to the sites studied already for bare surfaces, aluminol and mixed sites, also bridging sites were examined for uranyl adsorption where surface groups of neighboring kaolinite layers are simultaneously involved [107]. For both terminations of the (010) surface of kaolinite, aluminol and bridging sites were calculated to be energetically more favorable than mixed adsorption sites [107]. For some adsorption complexes, an aqua ligand of the first solvation shell of uranyl deprotonates, yielding uranyl monohydroxide as adsorbate, but this happened less frequently than on the bare edge surfaces (see above), most probably in consequence of additional stabilization due to solvation. Structurally, as for the bare edge surfaces, many adsorption complexes exhibit similar parameters (Table 16) [107]. This confirms the

Table 17. Optimized bulk parameters[a] of the primitive triclinic unit cell of selected 2:1 clay minerals. Distances in pm, angles in degrees.

Clay	*a*	*b*	*c*	*α*	*β*	*γ*
Pyro	522	907	985	91	100	90
Beidellite	523	907	1014	92	100	90
Beidellite, 8 H_2O	522	908	1328	93	101	90

(a) Energy cut-off 500 eV, (3×3×3) grid of k-points.

assumption that there should be several adsorption complexes in equilibrium on the surface [107].

In addition to U-Al/Si distances, EXAFS often is able to resolve two values of U-O_{eq}, ~230 and ~248 pm [211]. The shorter distance is interpreted as contacts to surface O atoms while the longer distance is tentatively assigned to the average distance to aqua ligands of the first solvation shell of uranyl [211]. Our computational study showed that there can be rather long distances to the surface as well as short U-O contacts to hydroxide ligands of uranium, formed by hydrolysis of adsorbed uranyl. Table 16 presents some examples of adsorption complexes that were calculated to be energetically preferred and exhibit long U-O contacts to the surface and short U-OH bonds. Comparison of various adsorption complexes reveals the trend that bonds to deprotonated surface O centers are short while contacts to surface OH groups are long. As some of the U-O_{surf} distances are of similar length as U-OH bonds, one cannot hope for an easy experimental discrimination. Rather, the interpretation of experimental data may be more complicated than commonly assumed.

4.2.3 Adsorption on 2:1 clay minerals

Common 2:1 clay minerals feature structural substitutions that result in charged layers, hence will require a more sophisticated modeling approach. Therefore, pyrophyllite with its neutral layers was chosen as starting point for modeling such 2:1 clay minerals. The chemical composition of pyrophyllite is $Al_4Si_8O_{20}(OH)_4$ [201]. Its basal surfaces offer only saturated oxygen centers; therefore, without charged substitutions, these basal surfaces can be assumed to be of minor importance for adsorbing ions such as uranyl. Thus, only adsorption on edge surfaces of pyrophyllite was studied [210]. Subsequently, as first approximation of more complex 2:1 clay minerals, a model of the charged clay mineral beidellite was constructed by exchanging one Al^{3+} ion per (2×1) unit cell for a Si^{4+} ion and adding one Na^+ counterion to the interlayer region. This model was applied to examine computationally the adsorption of uranyl on the basal and edge surfaces of beidellite.

Structure of 2:1 clay minerals: pyrophyllite and beidellite

The triclinic unit cell of pyrophyllite bulk was used when optimizing the bulk structure (Table 17). Two models of beidellite were optimized. First, a bare Na^+ counterion was used

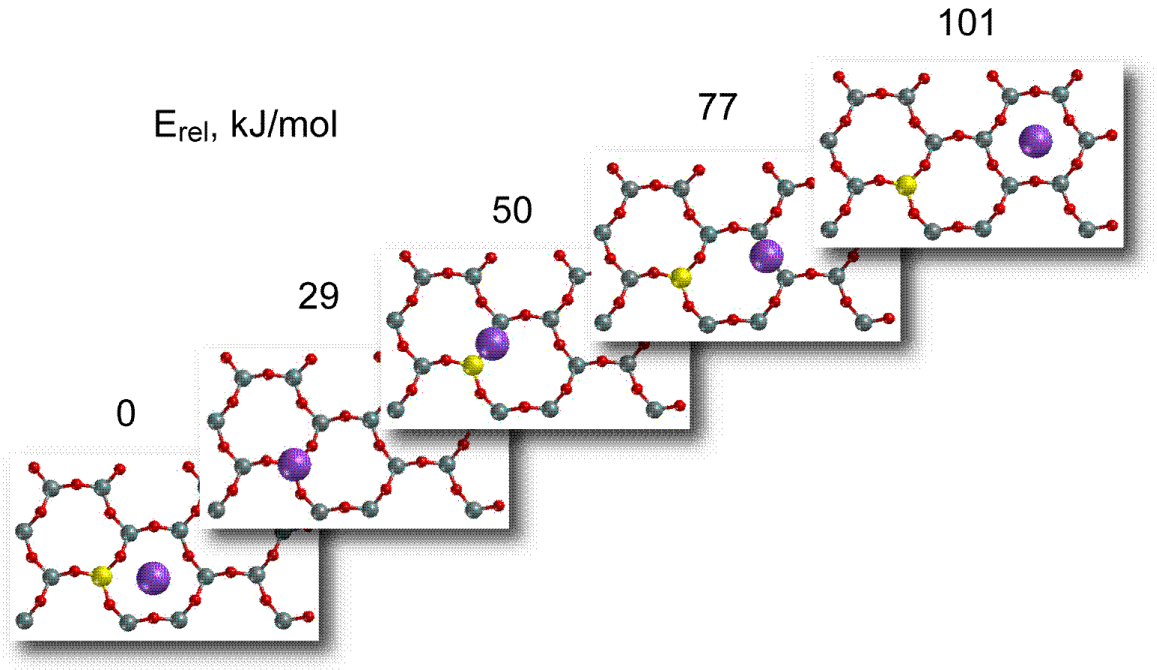

Figure 12. Relative positions of the counterion Na^+ (purple) with respect to the charged substitution on the surface (yellow) and the corresponding relative total energies in kJ mol^{-1}.

in the interlayer region; second, eight water molecules were added to approximate the solvation of the counter ion (Table 17).

The optimized bulk parameters obviously do not change much when one introduces a charged defect. Mainly, vector *c* is elongated. Pyrophyllite exhibits no counterions between the layers, thus vector *c* of its unit cell is shortest. A model of beidellite contains bare Na^+ as interlayer counterions and exhibits a vector *c* that is ~30 pm longer. Approximating solvation (swelling) by 8 water molecules per (2×1) unit cell of beidellite results in a vector *c* of 1328 pm which is considerably longer than that of pyrophyllite bulk (Table 17). As the other optimized bulk parameters do not change significantly, we used pyrophyllite bulk parameters in subsequent calculations when no explicit counter ion is present. This choice of the bulk parameters allows a direct comparison of neutral pyrophyllite and charged beidellite models. The basal surfaces of the 2:1 clay minerals studied were modeled by a monolayer. Thus, the interlayer spacing, reflecting mainly the length of vector *c*, is not important for such modeling.

The basal (001) surface of beidellite was described by a (2×2) unit cell of pyrophyllite with two substitutions of Si^{4+} by Al^{3+} in the upper Si(t) sheet to model the charge of 0.5 *e* per primitive unit cell (of pyrophyllite). The counterions Na^+ were placed at various positions relative to the charged substitution (Fig. 12). The most favorable position for Na^+ was determined in the $[(Al,Si_5)O_6]$ cavity next to the substitution (Fig. 12). Na^+ was modeled as inner-sphere complex solvated by three aqua ligands and as outer-sphere complex $Na(H_2O)_5^+$ adsorbed on the beidellite surface. The outer-sphere complex was

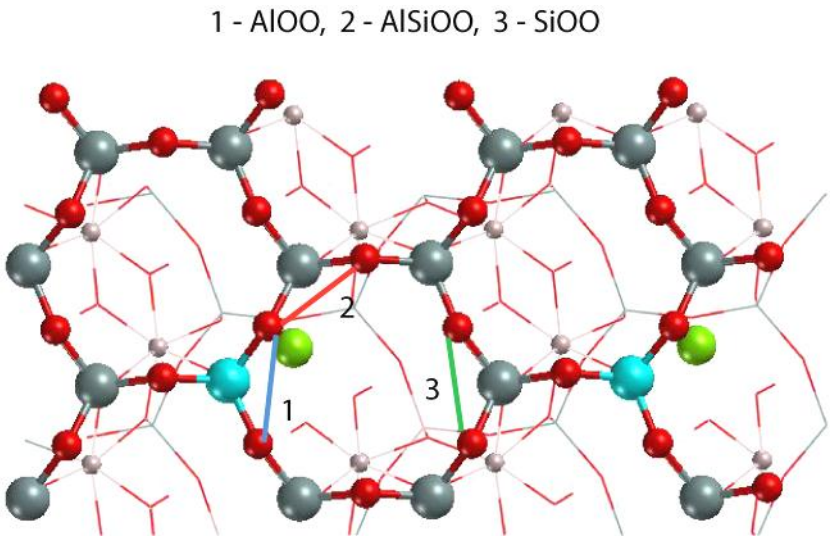

Figure 13. Possible bidentate adsorption sites for the uranyl ion on (001) beidellite surface. Substitution sites (Al^{3+}) in blue, counterions Na^{+} in green.

calculated 6 kJ mol^{-1} more favorable than the inner-sphere complex. Thus, a model of one layer pyrophyllite with two substitutions per (2×2) unit cell and two solvated counterions $Na(H_2O)_5^{+}$ adsorbed on the surface was used in the following for the (001) basal surface of beidellite.

Adsorption of uranyl(VI) on basal surfaces of beidellite

One of the adsorption mechanisms on 2:1 surface of clay minerals is ion exchange [195,215] where the positively charged counterions are exchanged by the adsorbate, uranyl in the present case. This type of adsorption was found to be prevailing for uranyl on montmorillonite at low pH values [195,215]. Experimentalists suggest that uranyl adsorbs as outer-sphere complex at low pH as only U-O_t and U-O_{eq} distances similar to those of the free uranyl ion were resolved in EXAFS experiments [195,215].

We studied inner-sphere bidentate and monodentate as well as outer-sphere adsorption complexes of uranyl on the basal (001) surface of our beidellite model. The adsorption sites on beidellite are shown in Fig. 13: SiOO (site 3), AlOO (site 1) at the substitution, and AlSiOO (site 2) which includes an O center connecting Si and Al atoms. A monodentate adsorption complex was modeled at the AlSiO center next to the substitution. We constructed two models for outer-sphere complexes, one above the substitution (model A) and one above the surface in between two substitutions (model B). Optimized structural parameters together with the relative energies are given in Table 18. Relative energies were calculated as formal reaction energies:

$$\text{Surf-}UO_2(H_2O)_n \rightarrow \text{Surf-}UO_2(H_2O)_{n-m} + m\ H_2O \qquad (10)$$

Table 18. Structural parameters[a] (in pm), relative energies E_{rel} estimated according to Eq. (10), and complex formation energies E_{form} estimated by Eq. (11) (in kJ mol^{-1}) for various adsorption complexes of uranyl on the bare basal surface of beidellite.

	Site	U-O_t	U-O_{Si}	U-O_{Al}	U-O_{eq}	U-Al	U-Si	E_{rel}	E_{form}
bi	1	179		245/252	249	311		50	199
	2	179	275	234	251	376	324	22	171
	3	178	255/268		251		328	50	199
mono		178		243	248	353	346	-20	129
	CN		U-OH						
outer[b] A	4	180	216		242			0	149
B	5	180	217		248			3	152
(4×2)[c] A	5	180	218		248				
Exp.[d]	5	179	218		241				

(a) U-O_t – uranyl bond, U-O_{Si} – U bonds to the surface O bound to Si centers, U-O_{Al} – uranyl bonds to surface O bound to Al cations, U-O_{eq} – average equatorial uranyl-ligand bond, U-Al – distance to surface Al center, U-Si – distance to surface Si center. (b) Model A: above the substitution, model B: between two substitutions. (c) Test case for a larger (4×2) unit cell with two substitutions. (d) EXAFS experiment at pH = 4.1, Ref. 195.

with an outer-sphere complex as reference. Formation energies of complexes (Table 18) were estimated as energies required for exchanging two solvated Na^+ counterions by one adsorbed uranyl ion:

$$\text{Surf-Na}_2(H_2O)_{10}^{2+} + UO_2(H_2O)_5^{2+} \rightarrow \text{Surf-UO}_2(H_2O)_n + (5\text{-}n)\ H_2O + 2\ Na(H_2O)_5^{+} \qquad (11)$$

In Eqs. (10) and (11), n = 3 for bidentate, n = 4 for monodentate, and n = 5 for outer-sphere complexes.

Bidentate coordinated species are energetically least favorable among all studied adsorption complexes on the (001) model beidellite surface (Table 18). They are 20-50 kJ mol^{-1} less stable than outer-sphere complexes. The monodentate species is calculated most stable, by 20 kJ mol^{-1} more stable than the outer-sphere species. Thus, it is unlikely that bidentate adsorption complexes of uranyl are favored on the (001) surface of beidellite. Also from experiment there is no hint on inner-sphere adsorption at the basal surfaces of 2:1 clay minerals. The favorable monodentate adsorption complex exhibits an uranyl bond U-O_t of 178 pm (Table 18) which has the same length as in the solvated uranyl ion. It also shows no splitting of the equatorial U-O bond lengths. The bond to the surface U-O_{surf} is 243 pm and the average U-O_{eq} is 248 pm, which is longer than the U-O_{eq} value for solvated UO_2^{2+}, 242 pm. Thus, the main structural parameters of the monodentate complex are similar to those of the solvated uranyl ion and thus may not easily be discriminated in EXAFS experiments. However, the complex also exhibits U-Al and U-Si distances of ~350 pm, distinguishing it from outer-sphere complexes. Yet, these relatively long contacts are hard to resolve in EXAFS experiments. We added one extra water molecule to the second solvation shell of

the adsorbed bidentate complex at site 2 to create a model with the same number of water molecules in the unit cell as for the monodentate complex. Direct comparison of the total energies of this model with the monodentate complex shows a slight preference for the latter one, by 8 kJ mol^{-1} only. Thus, taking into account the relatively small energy differences between preferred bidentate, monodentate, and outer-sphere species, these complexes may well coexist on basal surfaces of beidellite.

Outer-sphere complexes adsorbed on the (001) surface of beidellite tend to hydrolyze, yielding adsorbed uranyl monohydroxide. A proton from one of the aqua ligands of the first solvation shell of uranyl attaches to a surface O center. To check whether this is the result of the high charge of the beidellite layer (-0.5 *e* per primitive unit cell) we optimized the outer-sphere complex adsorbed in a (4×2) unit cell with two substitutions only, exhibiting a lower charge of -0.25 *e* per primitive unit cell of the slab. The results remained qualitatively similar. On the bare (001) surface of beidellite, outer-sphere complexes of uranyl mono-hydroxide with CN = 4 (model A) or CN = 5 (model B) were calculated, with a slight preference, 3 kJ mol^{-1}, for the first one. The outer-sphere complex A positioned above the substitution, initially created as five-fold coordinated, shows one rather large U-O_w bond of 293 pm and thus is classified as four-coordinate.

Surface solvation effects were approximately included in our models by adding about a water monolayer on the (001) surface of beidellite. For outer-sphere complexes we obtained again four- and five-coordinate species which hydrolyzed, but also a stable non-hydrolized species. Energy differences between these species were 10 kJ mol^{-1} at most. Thus, all these species may be present on the (001) surface of beidellite. As for uranyl on kaolinite (Section 4.2.2) we also modeled an outer-sphere complex, separated by two shells of water molecules from the surface. Also for this species we observed hydrolysis and calculated geometry parameters similar to the outer-sphere complexes in direct contact with the surface. Interestingly, this more distantly adsorbed outer sphere species is ~60 kJ mol^{-1} less stable than the outer-sphere species close to the surface. This result is no surprise as moving an uranyl outer-sphere complex away from the surface of a negatively charged mineral corresponds to a separation of charge.

Adsorption of uranyl(VI) on edge surfaces of pyrophyllite

The basal (001) surface is prevalent for crystallites of 2:1 clay minerals like pyrophyllite or beidellite. In addition, there are edge surfaces which exhibit unsaturated O centers that deprotonate at near neutral pH, creating negatively charged adsorption sites for actinide ions. They are assumed to be responsible for adsorption on 2:1 clay minerals at elevated pH values of solution [194,195,198,215]. There are several EXAFS experiments on uranyl adsorption on montmorillonite which show inner-sphere adsorption on edge surfaces at pH 5–8 [194,195,198,215]. We studied uranyl adsorption on (010) and (110) surfaces of pyrophyllite [210] and the (010) surface of beidellite (see below).

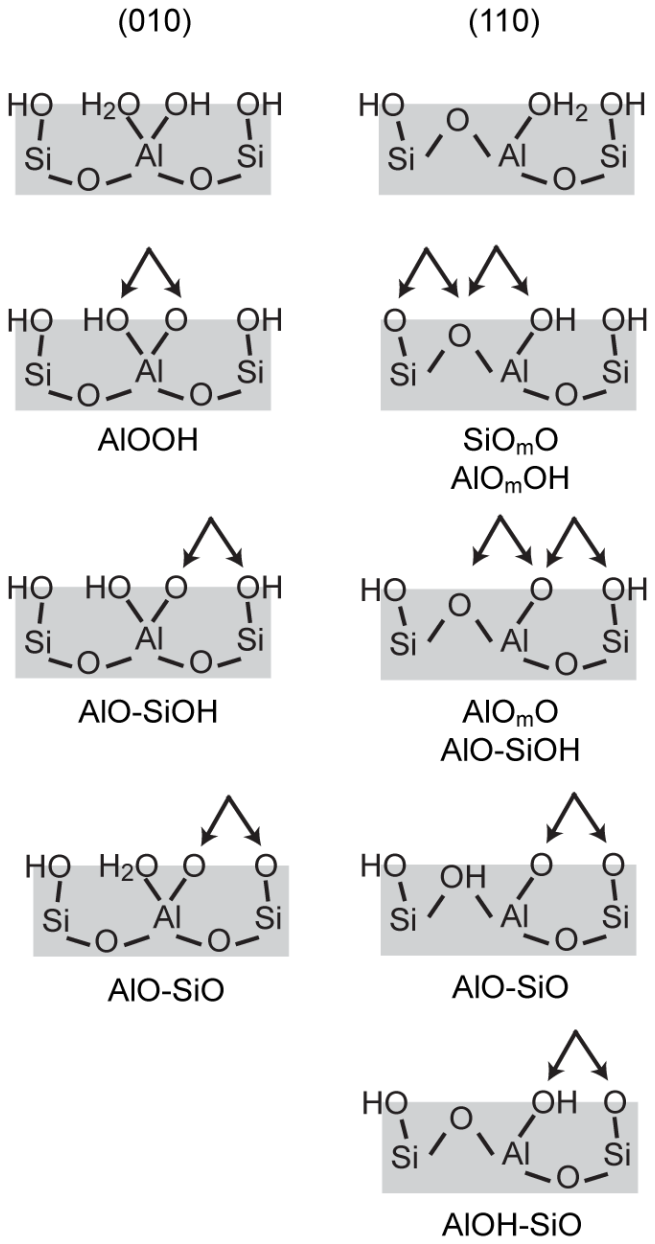

Figure 14. Adsorption sites on the (010) and (110) edge surfaces of pyrophyllite.

The structures of the (010) and (110) surfaces were created by cutting the pyrophyllite bulk along the weakest bonds and preserving the coordination numbers of Al and Si [210]. We examined only inner-sphere bidentate adsorption complexes on doubly deprotonated sites (q = -2 *e*) on the solvated edge surfaces of pyrophyllite [210] (Fig. 14). The (010) surface of pyrophyllite exhibits aluminol AlOOH sites and mixed AlO-SiO(H) sites. The (110) surface shows a larger variety of sites: aluminol sites $AlO_mO(H)$, silanol sites SiOO, and mixed sites AlO(H)-SiO(H) (Fig. 14). The aluminol sites on the (110) surface differ from the aluminol sites of the (010) surface as the former include mixed O_m centers bound to Si and Al ions, while the latter are formed by O centers bound to Al only.

The adsorption complexes on mixed sites of pyrophyllite edge surfaces converged to

Table 19. Calculated structural parameters[a] (in pm) and adsorption energies (in kJ mol^{-1}) of more favorable adsorption complexes of uranyl on solvated (010) and (110) surfaces of pyrophyllite. Experimental data for montmorillonite are given for comparison.

Site	$U\text{-}O_t$	$U\text{-}O_{surf}$	$U\text{-}O_W$	$U\text{-}O_{eq}$	U-Al/Si	ΔE_{form}
$[UO_2(H_2O)_{20}]^{2+}$	183			240		
(110)						
AlO_mO	185	211/239	245/247/253	240	328	137
AlO_mOH	182	233/243	229[b]/243/252	240	345	156
SiO_mO	181	231/240	246/247/262	245	302	198
AlOH-SiO	183	211/230	244/256	235	389/359	225
(010)						
AlO-SiO	185	211/225	243/245	231	362/340	149
AlOOH-SiOH[c]	185	208/252/261	245/257	245	327/349	210
Exp.						
UO_2^{2+} solv.[d]	176			241 (5)		
pH 5[e]	177			237 (5.7)	344	
pH 6.6[f]	179	229 (2.1)	247 (2.1)	238 (4.2)	331	
pH 7[g]	180	232 (2.8)	248 (2.1)	239 (4.9)	342	

(a) $U\text{-}O_t$ – uranyl bond, $U\text{-}O_{surf}$ – U bonds to the surface O, $U\text{-}O_W$ – uranyl bonds to aqua ligands, $U\text{-}O_{eq}$ – average equatorial uranyl-ligand bond, U-Al/Si – distance to surface Al/Si centers. (b) Bond length to OH ligand formed due to uranyl hydrolysis on the surface. (c) Tridentate coordination. (d) Data for solvated uranyl ion, Ref. 29. (e) Ref. 194. (f) Ref. 198. (g) Ref. 215. Experimental coordination numbers are given in parentheses.

4-coordinated uranyl. The complexes on aluminol and silanol sites kept coordination number 5. This result can be rationalized by the rather large $O_s\text{-}U\text{-}O_s$ angle, ~100°, of these sites, restricting the space for aqua ligands of uranyl [210]. In contrast to kaolinite, the adsorption on pyrophyllite leads less often to hydrolysis of adsorbed uranyl. Only one complex on the AlO_mOH site hydrolyzed (Table 19) [210].

Table 19 shows optimized structural parameters together with the complex formation energies for more favorable adsorption complexes on both surfaces [210]. Adsorption complexes on aluminol sites are most favorable on the (110) surface of pyrophyllite. Interestingly, uranyl adsorption on the (010) surface is favored at mixed AlO-SiO sites. We compared the trends for $U\text{-}O_t$ and $U\text{-}O_{eq}$ bond lengths for the solvated uranyl ion and the adsorbed uranyl ion, both observed in EXAFS [29,194,195,198,215] for montmorillonite and calculated with our models of pyrophyllite [210]. As proper reference, we optimized solvated uranyl with 20 water molecules, 5 of which modeled the first solvation shell, and another 15 were placed in the second solvation shell, as also the surface complexes included water molecules of the second shell. The $U\text{-}O_t$ bond converged to 183 pm, and $U\text{-}O_{eq}$ to 240 pm (Table 19). Adsorbed uranyl exhibits slightly elongated $U\text{-}O_t$ values and shorter or similar $U\text{-}O_{eq}$ values compared to a solvated uranyl ion at preferred sites. Similar trends are observed in experiment (Table 19). The calculated U-Al/Si distances of preferred

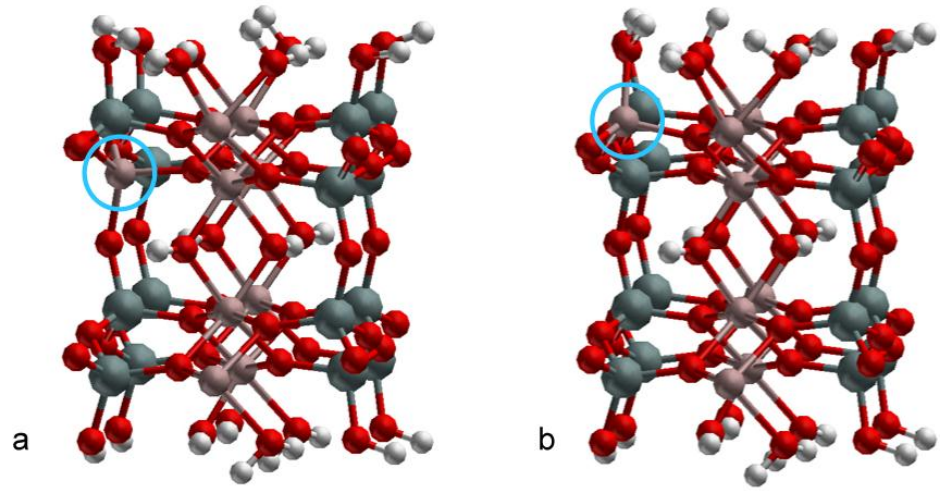

Figure 15. Structures of model beidellite (010) surfaces: (a) Defect Si^{4+} below the surface (modell A); (b) defect on the surface (model B).

complexes, 328–345 pm, fall in the range of the measured values, 331–344 pm [194,195,198,215].

The calculations showed that uranyl preferably adsorbs as five-coordinated complex on aluminol sites of the (110) surface of pyrophyllite, and as four-coordinated complex on mixed sites of the (010) surface [210]. This is at variance with the earlier assumption that uranyl adsorbs on Al (or Fe) octahedral sites [194,198]. It also shows that the adsorbed species on different edge facets may be characterized by different coordination numbers of uranyl. This is indirectly supported by fluorescence spectroscopy [216] as complexes with different CN of uranyl produce discernible spectra. We found several adsorption complexes on pyrophyllite that are close in energy and yield a distribution of key structural parameter similar to the corresponding EXAFS data. The most notable discrepancy between our computational results and EXAFS data is the coordination number of uranyl. While EXAFS determined CN mainly between 5 to 6 together with shorter U-O_{eq} values compared to solvated uranyl (CN = 5), we calculated for CN = 5 a tendency to elongated U-O_{eq} distances and for CN = 4 to shorter values than for solvated uranyl.

Adsorption of uranyl(VI) on edge surfaces of beidellite

(010) edge surfaces of a model 2:1 clay mineral with beidellitic substitution are constructed starting with the monoclinic structure of pyrophyllite as also other charged clay minerals show a monoclinic unit cell. Substitutions $Si^{4+} \rightarrow Al^{3+}$ are introduced below the surface layer (model A) or in the surface layer (model B) (Fig. 15). The charge of the substitutional defect is compensated by a proton attached to an aluminol group on the surface. In nature also short-range charge compensation is expected which either may be due to an adsorbed alkali ion or, at acidic conditions, due to a proton. Uranyl adsorption on these surfaces was examined at exemplary twofold deprotonated sites to achieve an overall neutral system. On pyrophyllite these are the most favored mixed site AlO-SiO and the AlOOH site (Table 21).

Table 20. Calculated structural parameters[a] (in pm) and complex formation energies (in kJ mol^{-1}) of adsorption complexes of uranyl on (010) edge surfaces of pyrophyllite and model beidellite.

Site		U-O_t	U-O_{surf}	U-O_W	U-O_{eq}	U-Al/Si	ΔE_{form}
$[UO_2(H_2O)_{20}]^{2+}$		183			240		
Pyrophyllite							
AlOOH		187	203/240	243/250/270	241	325	137
AlO-SiO		185	205/228	253/255	235	387/350	93
Beidellite[b]							
A	AlOHOH	184	222/236	241/245/257	240	345	155
	AlO-SiOH	186	199/262	246/265/271	249	386/390	84
B	AlOHOH	185	229/243	222[c]/244/250	238	348	115
	AlO-AlOH	187	201/244	248/265/274	246	386/390	23

(a) U-O_t – uranyl bond, U-O_{surf} – U bonds to the surface O, U-O_W – uranyl bonds to aqua ligands, U-O_{eq} – average equatorial uranyl-ligand bond, U-Al/Si – distance to surface Al/Si centers. (b) Modell A: Substitution below the surface; Modell B: Substitution on the surface (c) Bond length to OH ligand.

On the beidellitic model A, these sites change to AlO-SiOH and AlOHOH due to the proton compensating the defect charge. In view of the substitution at the surface the mixed site in model B corresponds to AlO-AlOH.

On the (010) edge surfaces of both models of beidellite uranyl adsorption at the mixed site AlO-SiOH and the corresponding site AlO-AlOH is more stable than at the aluminol sites, as already calculated for the (010) surface of pyrophyllite (Table 19). For the subsurface substitution in model A, uranyl is adsorbed slightly more strongly, by ~10 kJ mol^{-1}, at the favorite mixed site AlO-SiOH compared to pyrophyllite while substitution on the surface stabilized this surface complex by 70 kJ mol^{-1}. At the aluminol site a slight destabilization has to be noted for model A while the complex formation energies decreases by ~20 kJ mol for model B. Thus, a marked effect on the stability of the surface complex is only calculated when the substitutional defect lies close to the surface (Table 20).

Structure parameters seem to reflect more the effect of the extra charge compensating proton than that of the substitution. On pyrophyllite at the AlOOH site, a short contact of 203 pm to AlO and a longer one to AlOH of 240 pm is calculated. Thus, AlOHOH sites of the model beidellite show two longer contacts to oxygen atoms of the OH groups of 222-243 pm (Table 20). These bonds to the surface are longer on average; concomitantly, also the U-Al distance increases from 325 pm on pyrophyllite to 345 pm and 348 pm on the two model beidellite surfaces. For the mixed site AlO-SiO a shorter bond to the AlO group of 205 pm and a longer one of 228 pm to the SiO group is calculated for pyrophyllite (Table 20). For the corresponding sites AlO-SiOH and AlO-AlOH on the model beidellite again short bonds of ~200 pm to the AlO group are determined, while the bonds to the protonated groups

SiOH and AlOH are considerably elongated, to 262 pm and 244 pm, respectively. Again, the U-Al and U-Si distances follow these changes of the bonds to surface oxygen atoms. The distance U-Al remains essentially unchanged on going from pyrophyllite to model beidellite while U-Si elongates by 40 pm (Table 20).

Interesting results are calculated for the commonly measured parameter U-O_{eq}. For pyrophyllite a typical value of 240 pm is obtained for the AlOOH site and a smaller one, 235 pm, for the mixed site as a result of the reduced coordination, 4, of uranyl (Table 20). For the model beidellite the complexes at the AlOHOH site again show U-O_{eq} values typical for coordination number 5 while the mixed sites yield larger values of 246 pm and 249 pm.

4.3 Methodic topics

Modeling solvation effects is a key aspect when addressing the aqueous chemistry of actinides by computational methods. Quantifying solvation effects not only determines the accuracy of the results, but to a considerable extent also the computational effort. In the studies of solvated complexes reported above, the COSMO variant of the polarizable continuum model (PCM) approach [65,217] was applied throughout to account for long-range solvation effects. In PCM methods, the reaction field of the bulk solvent is represented typically via a charge density on the surface of a cavity around the solute. That cavity is constructed of sections of atom-centered spheres. The surface of this cavity is partitioned into spherical triangles (tessellation); to each such triangle a (point) charge is assigned as an element of the surface charge density. In the course of geometry optimizations, the cavity surface changes and spherical triangles, together with their assigned point charges, may not only move, but also appear or disappear discontinuously. Our experience showed, especially when carrying out geometry optimizations, that the well established GEPOL algorithm [218,219], used until now to construct the cavity, leads to discontinuous changes of the positions of the point charges on the cavity surface which implies small, yet noticeable discontinuities of the potential energy surface, hampering the optimization procedure. To achieve a smooth potential energy surface as function of the solute geometry, a weighting of the point charges by their distance to neighboring spheres has been implemented, following the recently developed "fixed point charge with variable area" algorithm (FIXPVA) [220]. This algorithm is numerically much more stable and furnishes more accurate components due to solvation of the forces acting on the atoms of the solute. Ultimately, one observes a more stable and more efficient optimization procedure. As the FIXPVA procedure tends to underestimate the solvent excluded surface around a solute [220], implying an underestimation of solvation energies, it seemed appropriate to adjust the scaling factor of the atomic radii used to construct the cavity. In this way slightly improved values of the solvation energies were obtained from a numerically more stable optimization procedure (Table 21). For a test set of 7 cations and 8 anions, the deviation

Table 21. Solvation free energies calculated with the GEPOL and the FIXPVA tessellation schemes. Experimental values are shown for comparison. Energies in kJ mol^{-1}.

	GEPOL	FIXPVA	Exp.
H_2O	28	31	26[a]
$[H_3O]^+$	378	377	427[b]
OH^-	378	400	430[c]
CH_3COOH	22	25	25[a]
$[CH_3COO]^-$	274	286	365[c]
UO_2^{2+}	1249	1345	1347[d], 1682[e]

(a) Ref. 222, (b) Ref. 223, (c) Ref. 223, (d) Ref. 224, (e) Ref. 225

from experimental solvation energies was be reduced by ~30 %, while essentially no change was observed for neutral species.

As an alternative to the rather accurate periodic plane-wave and PAW approach (software VASP, see Section 2) used in this project, the potential of an efficient Γ-point periodic plane-wave approach together with norm-conserving pseudopotentials as implemented in the software NWChem [226] was explored. Results of density functional GGA calculations for the uranyl(VI) aqua complex, kaolinite bulk as well as uranyl adsorbed at the AlOO site of the (001) Al(o) surface of kaolinite agreed well with the corresponding VASP calculations. As a trend, the uranyl bond was underestimated by ~3 pm in all calculations, in agreement with other computational studies [89] while ligand bonds were reproduced more accurately. No gain in computational efficiency was observed for NWChem compared to VASP for small test systems. Yet, we noted a more favorable scaling with increasing numbers of processors which makes this software interesting for large systems and dynamical simulations.

To examine and partially correct self-interaction artifacts of DF LDA and GGA approaches in calculations of actinide complexes, we implemented the DFT+U method in our software ParaGauss [227] and parameterized it for uranium [136]. In this empirical approach a Hubbard like repulsion term is added to the interaction of f-electrons, favoring localized f-orbitals. U parameters of 1-2 eV have been determined to be reasonable for uranium by comparison of calculated to experimental ionization potentials of UO and UO_2. Self-interaction artifacts have been characterized for uranyl(VI) [136] and its mono-hydroxide [135] (Section 4.1.1). Our results demonstrate that these artifacts are more pronounced in the gas phase than in solution and that the DFT+U approach removes these artifacts to a considerable extent.

5 Summary

A detailed mechanistic understanding of actinide chemistry under environmental conditions is an important prerequisite for modeling and predicting speciation, distribution, and migration of actinides in the environment. These issues are of key importance in safety

considerations of long-term storage of highly radioactive waste in underground repositories. In this project quantum chemical computational were used to study the chemistry of actinides in solution and at clay mineral surfaces to complement pertinent experimental work. Quantum chemical studies, together with spectroscopic experiments, offer the unique opportunity to gain insight at the atomic level and thus are useful for identifying species and developing mechanistic models of actinide chemistry under pertinent conditions. Two relevant aspects of actinide environmental chemistry have been treated in this project: complexation in aqueous solution by inorganic and organic ligands and the interaction of actinide ions and complexes with surfaces of clay minerals.

Complexes of actinyl ions with small organic ligands have been examined as models of actinyl complexation by functional groups of humic substances with the goal to characterize how groups beyond carboxyl functions contribute to the ability of humic substances to form complexes with metal ions. In agreement with experimental studies we showed that sulfonate, amine, and pyridine groups are not important for actinyl complexation in comparison to the prevailing carboxyl groups. A study of ternary hydroxo-acetate complexes of uranyl(VI) revealed that these complexes should be less stable than binary acetate complexes, in contrast to the interpretation of measured values of pertinent complexation constants. Thus, complexation with carboxyl functional groups at neutral to basic conditions in competition with hydrolysis raises still some questions. For the exemplary case of uranyl complexation with an acetate ligand we demonstrated that the weak increase in the complexation constant with increasing temperature has to be ascribed to a bidentate isomer and that the equilibrium between mono- and bidentate isomers of uranyl acetate is influenced by temperature. This result also showed that a fundamental understanding of actinide complexation needs to take into account the equilibrium between various isomers of a complex of given composition, a topic studied only rarely until now. Preliminary examination of the reaction mechanism of neptunyl(V) with acetate supports this view. By model calculations on Am(III) aqua and monoacetate complexes we contributed to the understanding of this rarely treated element. Finally we examined the first hydrolysis products of U(VI), U(IV), and Np(IV), providing structural and energetic parameters for these experimentally not easily accessible species.

Quantum chemical modeling of actinide adsorption at mineral surfaces was pioneered by our group and detailed studies of actinyl adsorption on clay minerals surfaces have been carried out in this project. Our results for basal and edge surfaces of kaolinite confirm the interpretation of pertinent EXAFS experiments regarding bidentate adsorption complexes of uranyl(VI). However, detailed comparison of geometries and energies revealed that mono-dentate coordination to the surface can not be excluded. Also, we were unable to identify clearly preferred sites for adsorption, thus various adsorption complexes may coexist.

Besides adsorbed uranyl, we also obtained uranyl hydroxide as adsorbate in our model calculations.

Comparison of structural parameters to available experimental data showed that the current interpretation of measured U-O distances to ligands and to the surface should be extended. Shorter U-O bonds have been ascribed to bonds to the surface while longer ones were ascribed to aqua ligands. We calculated also rather short bonds of U to hydroxide ligands and relatively long ones, comparable to bonds to aqua ligands, to protonated surface groups. Similar results as for kaolinite were obtained for adsorbed uranyl on edge surfaces of pyrophyllite and a model beidellite. While aluminol sites are preferred for kaolinite and the (110) edge surface of pyrophyllite, we determined a mixed aluminol-silanol site to be favorable on the (010) edge surface of pyrophyllite. Thus, preferred adsorption sites seem to depend on the exposed surface. Examination of the basal surface of beidellitic substituted pyrophyllite provided another example of a surface of a clay mineral where several adsorption complexes may coexist, as we calculated rather small differences in adsorption energies for inner- and outer-sphere complexes of uranyl.

All these examples demonstrated that actinide-clay adsorption systems are rather complex at the atomic level, featuring a variety of surface species which are not easily discriminated. Further computational as well as spectroscopic studies are necessary to develop a mechanistic model at environmental conditions to construct a basis for the interpretation of experimental results. Especially infrared spectroscopy and resonant anomalous X-ray reflectivity techniques will be helpful in this regard, besides quantum chemical studies, to complement available microscopic information.

6 Publications Resulting from this Project

1) R. Ramakrishnan, A. V. Matveev, S. Krüger, N. Rösch; Self-Interaction Artifacts on Structural Features of Uranyl Monohydroxide from Kohn-Sham Calculations. Theor. Chem. Acc. 130, 361-369 (2011).
2) O. Zakharieva, A. Kremleva, S. Krüger, N. Rösch; Uranyl Complexation by Monodentate Nitrogen Donor Ligands. A Relativistic Density Functional Study, Int. J. Quantum Chem. 211, 2045-2053 (2011).
3) A. Kremleva, S. Krüger, N. Rösch; Uranyl Adsorption at (010) Edge Surfaces of Kaolinite. A Density Functional Study, Geochim. Cosmochim. Acta 75, 706-718 (2011).
4) R. Ramakrishnan, A. V. Matveev, N. Rösch; Effects of the Self-Interaction Error in Kohn-Sham Calculations: A DFT+U Case Study on Penta-Aqua Uranyl(VI), Comp. Theor. Chem. 963, 337-343 (2011).
5) R. Ramakrishnan, The DFT+U Method in the Framework of the Parallel Density Functional Code ParaGauss, Dissertation, Technische Universität München, 2011.
6) A. Kremleva, S. Krüger, N. Rösch; Quantum Chemical Modeling of Uranyl Adsorption on Mineral Surfaces, Radiochim. Acta 98, 635-646 (2010).

7) B. Martorell, A. Kremleva, S. Krüger, N. Rösch; Density Functional Model Study of Uranyl Adsorption on the Solvated (001) Surface of Kaolinite, J. Phys. Chem. C 114, 13287–13294 (2010).

8) F. Schlosser, L. V. Moskaleva, A. Kremlevea, S. Krüger, N. Rösch; Comparative Density Functional Study of the Complexes $[UO_2(CO_3)_3]^{4-}$ and $[(UO_2)_3(CO_3)_6]^{6-}$ in Aqueous Solution, Dalton Trans. 5705-5712 (2010).

9) R. S. Ray, S. Krüger, N. Rösch; Ternary Uranyl Hydroxo Complexes: A Computational Study of Structure, Energetics, and Stability Constants, Inorg. Chim. Acta 363, 263-269 (2010).

10) R. S. Ray, S. Krüger, N. Rösch; Uranyl Monocarboxylates of Aromatic Acids: A Density Functional Model Study of Uranyl Humate Complexation, Dalton Trans. 3590–3598 (2009).

11) A. Kremleva, S. Krüger, N. Rösch; Role of Aliphatic and Phenolic Hydroxyl Groups in Uranyl Complexation by Humic Substances, Inorg. Chim. Acta 362, 2542–2550 (2009).

12) A. Kremleva, Environmental Chemistry of Uranyl: A Relativistic Density Functional Study on Complexation with Humic Substances and Sorption at Kaolinite, Dissertation, Technische Universität München, 2009.

13) R. S. Ray, A Relativistic Density Functional Study of Uranyl Hydrolysis and Complexation by Carboxylic Acids in Aqueous Solution, Dissertation, Technische Universität München, 2009.

14) Y. Zhang, A Density Functional Study of Uranyl Complexation by Sulfur Containing Humic Acids in Aqueous Solution, Master Thesis, Technische Universität München, 2009.

15) A. Kremleva, S. Krüger, N. Rösch; Density Functional Model Studies of Uranyl Adsorption on (001) Surfaces of Kaolinite, Langmuir 24, 9515-9524 (2008).

16) N. Rösch, S. Krüger; Plane Wave Density Functional Model Studies of Chemistry at Surfaces, in: High Performance Computing in Science and Engineering, Transactions of the Third Joint HLRB and KONWIHR Result and Status Workshop, Garching 2007, S. Wagner, M. Steinmetz, A. Bode, M. Brehm (eds.), Springer: Berlin, 2008, pp. 173-186.

17) C. Chiu, Density Functional Studies on Uranyl Complexation bz Amino Acids, Bachelor Thesis, Technische Universität München, 2008.

Further publications on results of this project and follow-up studies are in preparation.

7 References

[1] J. J. Katz, G. T. Seaborg, L.R. Morss (Eds.), The Chemistry of the Actinide Elements, 2. ed., Chapman and Hall, New York, 1986.

[2] L. R. Morss, N. M. Edelstein, J. Fuger (Eds.), Actinide and Transactinide Elements, 3. ed., Springer, Dordrecht, 2006.

[3] Z. Szabo, T. Toraishi, V. Vallet, I. Grenthe, Coord. Chem. Rev. 250 (2006) 784.

[4] Ref. 2, vol. 4, chap. 22.

[5] D. L. Clark, D. E. Hobart, M. P. Neu, Chem. Rev. 95 (1995) 25.

[6] K. H. Lieser, Radiochim. Acta 70/71 (1995) 355.
[7] R. J. Silva, H. Nitsche, Radiochim. Acta 70/71 (1995) 377.
[8] Ref. 2, vol. 4, chap. 23.
[9] F. J. Stevenson, Humus Chemistry, 2. ed., Wiley, New York, 1994.
[10] K. L. Nash, J. M. Cleveland, T. F. Rees, J. Environ. Radioact. 7 (1988) 131.
[11] G. R. Choppin, Radiochim. Acta 44/45 (1988) 23.
[12] M. A. Denecke, S. Pompe, T. Reich, H. Moll, M. Bubner, K. H. Heise, R. Nicolai, H. Nitsche, Radiochim. Acta 79 (1997) 151.
[13] S. Sachs, K. Schmeide, T. Reich, V. Brendler, K. H. Heise, G. Bernhard, Radiochim. Acta 93 (2005) 17.
[14] K. Schmeide, T. Reich, S. Sachs, V. Brendler, K. H. Heise, G. Bernhard, Radiochim. Acta 93 (2005) 187.
[15] M. A. Denecke, T. Reich, S. Pompe, M. Bubner, K. H. Heise, H. Nitsche, P. G. Allen, J. J. Bucher, N. M. Edelstein, D. K. Shuh, J. Phys. IV 7 C2 (1997) 637.
[16] S. Pompe, K. Schmeide, M. Bubner, G. Geipel, K. H. Heise, G. Bernhard, H. Nitsche, Radiochim. Acta 88 (2000) 553.
[17] K. Schmeide, S. Sachs, M. Bubner, T. Reich, K. H. Heise, G. Bernhard, Inorg. Chim. Acta 351 (2003) 133.
[18] S. Sachs, G. Bernhard, Radiochim. Acta 93 (2005) 141.
[19] S. Pompe, M. Bubner, M. A. Denecke, T. Reich, A. Brachmann, G. Geipel, R. Nicolai, K. H. Heise, H. Nitsche, Radiochim. Acta 74 (1996) 135.
[20] M. A. Denecke, Coord. Chem. Rev. 250 (2006) 730.
[21] R. Steudtner, K. Müller, K. Schmeide, S. Sachs, G. Bernhard, Dalton Trans. 40 (2011) 11920.
[22] R. N. Collins, T. Saito, N. Aoyagi, T. E. Payne, T. Kimura, T. D. Waite, J. Env. Qual. 40 (2011) 731.
[23] S. Pompe, A. Brachmann, M. Bubner, G. Geipel, K. H. Heise, G. Bernhard, H. Nitsche, Radiochim. Acta 82 (1998) 89.
[24] V. Vallet, Z. Szabó, I. Grenthe, Dalton Trans. (2004) 3799.
[25] V. Vallet, P. Macak, U. Wahlgren, I. Grenthe, Theor. Chem. Acc. 115 (2006) 145.
[26] Ref. 2, vol. 3, chap. 17.
[27] H. Moll, G. Geipel, T. Reich, G. Bernhard, T. Fanghänel, I. Grenthe, Radiochim. Acta 91 (2003) 11.
[28] J. Jiang, L. Rao, P. Di Bernardo, P. L. Zanonato, A. Bismondo, J. Chem. Soc., Dalton Trans. 8(2002) 1832.
[29] P. G. Allen, J. J. Bucher, D. K. Shuh, N. M. Edelstein, T. Reich, Inorg. Chem. 36 (1997) 4676.
[30] T. Schäfer, R. Michel, F. Claret, Journal of Physics: Conf. Series 186 (2009) 012095.
[31] T. Schäfer, R. Michel, F. Claret, T. Beetz, R. Wirick, C. Jacobsen, J. Electron Spec. Rel. Phenomena 170 (2009) 49.
[32] P. Benes, K. Kratzer, S. Vlckova, E. Sebestova, Radiochim. Acta 82 (1998) 367.
[33] A. Krepelova, S. Sachs, G. Bernhard, Radiochim. Acta 94 (2006) 825.
[34] R. Kautenburger, H. P. Beck, ChemSusChem 1 (2008) 295.

[35] C. Joseph, K. Schmeide, S. Sachs, V. Brendler, G. Geipel, G. Bernhard, Chem. Geol. 284 (2011) 240.

[36] M. H. Lee, E. C. Jung, K. Song, Y. H. Han, H. S. Shin, J. Radioanal. Nuc. Chem. 287 (2011) 639.

[37] E. A. Jenne (Ed.), Adsorption of Metals by Geomedia: Variables, Mechanisms and Model Applications, Academic Press, United Kingdom, 1998.

[38] M. Barnett, D. Kent (Eds.), Adsorption of Metals by Geomedia II: Variables, Mechanisms, and Model Applications, Elsevier, USA, 2008.

[39] H. Geckeis, T. Rabung, J. Cont. Hydrol. 102 (2008) 187.

[40] K. Choi, J. W. Park, Geoscience J. 9 (2005) 53.

[41] S. S. Lee, P. Fenter, C. Park, N. C. Sturchio, K. L. Nagy, Langmuir 26 (2010) 16647.

[42] P. Fenter, S. S. Lee, C. Park, L. Soderholm, R. E. Wilson, O. Schwindt, Geochim. Cosmochim. Acta 74 (2010) 6984.

[43] A. Kremleva, S. Krüger, N. Rösch, Radiochim. Acta 98 (2010) 635.

[44] G. Kresse, J. Furthmüller, Phys. Rev. B 54 (1996) 11169.

[45] G. Kresse, J. Hafner, Phys. Rev. B 49 (1994) 14251.

[46] G. Kresse, J. Hafner, Phys. Rev. B 47 (1993) 558.

[47] G. Kresse, J. Hafner, Phys. Rev. B 48 (1993) 13115.

[48] G. Kresse, J. Furthmüller, Comput. Mater. Sci. 6 (1996) 15.

[49] G. Kresse, D. Joubert, Phys. Rev. B 59 (1999) 1758.

[50] A. H. MacDonald, S. H. Vosko, J. Phys. C 12 (1979) 2977.

[51] W. Koch, M. C. Holthausen, A Chemist's Guide to Density Functional Theory, 2. ed. Wiley-VCH, Weinheim, 2000.

[52] T. Ziegler, Chem. Rev. 91 (1991) 651.

[53] J. P. Perdew, A. Zunger, Phys. Rev. B 23 (1981) 5048.

[54] J. P. Perdew, Y. Wang, Phys. Rev. B 45 (1992) 13244.

[55] L. V. Moskaleva, V. A. Nasluzov, N. Rösch, Langmuir 22 (2006) 2141.

[56] F. Schlosser, S. Krüger, N. Rösch, Inorg. Chem. 45 (2006) 1480.

[57] A. Kremleva, S. Krüger, N. Rösch, Inorg. Chim. Acta 362 (2009) 2542.

[58] R. S. Ray, S. Krüger, N. Rösch, Dalton Trans. (2009) 3590.

[59] N. Rösch, S. Krüger, M. Mayer, V. A. Nasluzov, The Douglas-Kroll-Hess Approach to Relativistic Density Functional Theory: Methodological Aspects and Applications to Metal Complexes and Clusters, in: Recent Developments and Applications of Modern Density Functional Theory, J. M. Seminario (Eds.), Theoretical and Computational Chemistry Series, vol. 4, Elsevier, Amsterdam, 1996, p. 497.

[60] N. Rösch, A. V. Matveev, V. A. Nasluzov, K. M. Neyman, L. Moskaleva, S. Krüger, Quantum Chemistry with the Douglas-Kroll-Hess Approach to Relativistic Density Functional Theory: Efficient Methods for Molecules and Materials, in: Relativistic Electronic Structure Theory-Applications, P. Schwerdtfeger (Ed.) Theoretical and Computational Chemistry Series, Elsevier, Amsterdam, 2004, p. 656.

[61] T. Belling, T. Grauschopf, S. Krüger, F. Nörtemann, M. Staufer, M. Mayer, V. A. Nasluzov, U. Birkenheuer, A. Hu, A. V. Matveev, A. M. Shor, M. Fuchs-Rohr, K. Neyman, D. I. Ganyushin, T. Kerdcharoen, A. Woiterski, A. Gordienko, S. Majumder, N. Rösch, ParaGauss, Version 3.0, Technische Universität München, 2004.

[62] S. H. Vosko, L. Wilk, M. Nusair, Can. J. Chem. 58 (1980) 1200.
[63] A. D. Becke, Phys. Rev. A 38 (1988) 3098.
[64] J. P. Perdew, Phys. Rev. B 33 (1986) 8822.
[65] M. S. K. Fuchs, A. M. Shor, N. Rösch, Int. J. Quantum Chem. 86 (2002) 487.
[66] G. Schreckenbach, G. A. Shamov, Accounts Chem. Res. 43 (2010) 19.
[67] V. Vallet, I. Grenthe, Comptes Rendus Chimie 10 (2007) 905.
[68] F. Ruiperez, C. Danilo, F. Real, J. P. Flament, V. Vallet, U. Wahlgren, J. Phys. Chem. A 113 (2009) 1420.
[69] B. A. Hess (Ed.), Relativistic Effects in Heavy Element Physics and Chemistry, Wiley, Chichester, 2003, chap. 3.
[70] X. Cao, M. Dolg, Coord. Chem. Rev. 250 (2006) 900.
[71] S. O. Odoh, G. Schreckenbach, J. Phys. Chem. A 114 (2010) 1957.
[72] E. van Lenthe, E. J. Baerends, J. G. Snijders, J. Chem. Phys. 99 (1993) 4597.
[73] G. A. Shamov, G. Schreckenbach, J. Phys. Chem. A 109 (2005) 10961.
[74] J. Su, L. Zhang, W. H. E. Schwarz, J. Li, Inorg. Chem. 50 (2011) 2082.
[75] D. Paez-Hernandez, J. A. Murillo-Lopez, R. Arratia-Perez, J. Phys. Chem. A 105 (2011) 8997.
[76] L. V. Moskaleva, S. Krüger, A. Spörl, N. Rösch, Inorg. Chem. 43 (2004) 4080.
[77] M. Garcia-Hernandez, C. Lauterbach, S. Krüger, A. Matveev, N. Rösch, J. Comp. Chem. 23 (2002) 834.
[78] C. Clavaguéra-Sarrio, V. Vallet, D. Maynau, C. J. Marsden, J. Chem. Phys. 121 (2004) 5312.
[79] E. Fromager, V. Vallet, B. Schimmelpfennig, P. Macak, T. Privalov, U. Wahlgren, J. Phys. Chem. A 109 (2005) 4957.
[80] J. Tomasi, B. Mennucci, R. Cammi, Chem. Rev. 105 (2005) 2999.
[81] C. J. Cramer, D. G. Truhlar, Acc. Chem. Res. 41 (2008) 760.
[82] M. Bühl, G. Wipff, Chem. Phys. Chem. 12 (2011) 3095.
[83] Z. Cao, K. Balasubramanian, J. Chem. Phys. 123 (2005) 114309.
[84] K. E. Gutkowski, D. A. Dixon, J. Phys. Chem. A 110 (2006) 8840.
[85] B. Siboulet, C. J. Marsden, P. Vitorge, Chem. Phys. 326 (2006) 289.
[86] P. Wahlin, B. Schimmelpfennig, U. Wahlgren, I. Grenthe, V. Vallet, Theor. Chem. Acc. 124 (2009) 377.
[87] V. Vallet, U. Wahlgren, B. Schimmelpfennig, H. Moll, Y. Szabó, I. Grenthe, Inorg. Chem. 40 (2001) 3516.
[88] R. Car, M. Parrinello, Phys. Rev. Lett. 55 (1985) 2471.
[89] P. Nichols, E. J. Bylaska, G. K. Schenter, W. de Jong, J. Chem. Phys. 128 (2008) 124507.
[90] R. Atta-Fynn, E. J. Bylaska, G. K. Schenter, W. A. de Jong, J. Phys. Chem. A 115 (2011) 4665.
[91] V. A. Cocalia, K. E. Gutowski, R. D. Rogers, Coord. Chem. Rev. 250 (2006) 755.
[92] I. Infante, B. van Stralen, L. Vischer, J. Comp. Chem. 27 (2006) 1156.
[93] Y. Hagiwara, M. Tateno, J. Phys. Cond. Mat. 22 (2010) 413101.

[94] S. Difley, L.-P. Wang, S. Yeganeh, S. R. Yost, T. Van Voorhis, Acc. Chem Res. 43 (2010) 995

[95] A. Genest, A. Woiterski, S. Krüger, A. Shor, N. Rösch, J. Chem. Theory Comput. 2 (2006) 47.

[96] A. Shor, S. Krüger, N. Rösch, unpublished results.

[97] I. Infante, L. Vischer, J. Comp. Chem. 25 (2004) 386.

[98] R. Spezia, B. Siboulet, S. Abadie, R. Vuilleumier, P. Vitorge, J. Phys. Chem. B 115 (2011) 3560.

[99] S. Tsushima, J. Phys. Chem. B 112 (2008) 7080.

[100] A. Ikeda-Ohno, S. Tsushima, K. Takao, A. Rossberg, H. Funke, A. C. Scheinost, G. Bernhard, T. Yaita, C. Hennig, Inorg. Chem. 48 (2009) 11779.

[101] S. O. Odoh, G. Schreckenbach, J. Phys. Chem. A 115 (2011) 14110.

[102] X. Tan, M. Fang, X. Wang, Molecules 15 (2010) 8431.

[103] L. V. Moskaleva, V. A. Nasluzov, N. Rösch, Langmuir 22 (2006) 2141.

[104] H. Perron, C. Domain, J. Roques, R. Drot, E. Simoni, H. Catalette, Inorg. Chem. 45 (2006) 6568.

[105] A. Kremleva, S. Krüger, N. Rösch, Langmuir 24 (2008) 9515.

[106] B. Martorell, A. Kremleva, S. Krüger, N. Rösch, J. Phys. Chem. C 114 (2010) 13287.

[107] A. Kremleva, S. Krüger, N. Rösch, Geochim. Cosmochim. Acta 75 (2011) 706.

[108] E. Veilly, J. Roques, M.-C. Jodin-Caumon, B. Humbert, R. Drot, E. Simoni, J. Chem. Phys. 129 (2008) 244704.

[109] J. Roques, E. Veilly, E. Simoni, Int. J. Mol. Sci. 10 (2009) 2633.

[110] D. M. Sherman, C- L. Peacock, C. G. Hubbard, Geochim. Cosmochim. Acta 72 (2008) 298.

[111] T. Hattori, T. Saito, K. Ispida, A. C. Scheinost, T. Tsuneda, S. Nagasaki, S. Tanaka, Geochim. Cosmochim. Acta 73 (2009) 5975.

[112] R. Polly, B. Schimmelpfennig, R. Rabung, M. Flörsheimer, R. Klenze, H. Geckeis, , Radiochim. Acta 98 (2010) 627.

[113] V. A. Glezakou, W. A. de Jong, J. Phys. Chem. A 115 (2011) 1257

[114] L. C. Shuller, J. Poling, R. C. Ewing, U. Becker, Geochim. Cosmochim. Acta 72 (2008) A864.

[115] C. Benzi, A. Kremleva, S. Krüger, N. Rösch, in preparation.

[116] S. V. Churakov, Geochim. Cosmochim. Acta 71 (2007) 1130.

[117] M. Flörsheimer, K. Kruse, R. Polly, A. Abdelmonem, B. Schimmelpfennig, R. Klenze, T. Fanghänel, Langmuir 24 (2008) 13434.

[118] D. Tunega, M. H. Gerzabek, H. Lischka, J. Phys. Chem. B 108 (2004) 5930.

[119] R. S. Ray, S. Krüger, N. Rösch, in preparation.

[120] Ref. 2, vol. 1, chap. 5.10.2.

[121] I. Grenthe, J. Fuger, R. J. M. Konigs, R. J. Lemire, A. B. Muller, C. Nguyen-Trung, H. Wanner, Chemical Thermodynamics of Uranium, vol. 1., Elsevier Science, North-Holland, Amsterdam, 1992.

[122] V. Eliet, G. Bidoglio, N. Omenetto, L. Parma, I. Grenthe, J. Chem. Soc., Faraday Trans. 91 (1995) 2275.

[123] P. L. Brown, Radiochim. Acta 90 (2002) 589.
[124] F. Quiles, C. Nguyen-Trung, C. Carteret, B. Humbert, Inorg. Chem. 50 (2011) 2811.
[125] P. J. Hay, R. L. Martin, G. Schreckenbach, Phys. Chem. A. 104 (2000) 6259.
[126] M. Druchok, T. Bryk, M. Holovko, J. Mol. Liq. 120 (2005) 11.
[127] M. Bühl, H. Kabrede, ChemPhysChem. 7 (2006) 2290.
[128] K. I. M. Ingram, L. J. L. Haller, N. Kaltsoyannis, Dalton Trans. (2006) 2403.
[129] Y. Oda, A. Aoshima J. Nucl. Sci. Techno. 39 (2002) 647.
[130] S. Tsushima, T. Yang, A. Suzuki, Chem. Phys. Lett. 334 (2001) 365.
[131] C. Nguyen-Trung, D. A. Palmer, G. M. Begun, C. Peiffert, R. E. Mesmer, J. Soln. Chem. 29 (2000) 101.
[132] F. Quiles, A. Burneau, Vibr. Spectros. 18 (1998) 61.
[133] C. F. Baes Jr., R. E. Mesmer, The Hydrolysis of Cations, J. Wiley & Sons, New York, 1976; pp. 174-182.
[134] V. Eliet, G. Bidoglio, N. Omenetto, L. Parma, I. Grenthe, J. Chem. Soc., Faraday Trans. 91 (1995) 2275.
[135] R. Ramakrishnan, A. V. Matveev, S. Krüger, N. Rösch, Theor. Chem. Acc. 130 (2011) 361.
[136] R. Ramakrishnan, A. V. Matveev, N. Rösch, Comp. Theor. Chem. 963 (2011) 337.
[137] Z. Szabo, H. Moll. I. Grenthe, J. Chem Soc. Dalton Trans. 18 (2000) 3158.
[138] P. Zeh, K. R. Czerwinski, J. I. Kim, Radiochim. Acta 76 (1997) 37.
[139] I. Pashalidis, G. Buckau, J. Radioanal. Nucl. Chem. 273 (2007) 315.
[140] S. Sachs, V. Brendler, G. Geipel, Radiochim. Acta 95 (2007) 103.
[141] P. Panak, R. Klenze, J. I. Kim, Radiochim. Acta 74 (1996) 141.
[142] M. Morgenstern, R. Klenze, J. I. Kim, Radiochim. Acta 56 (1992) 79.
[143] R. S. Ray, S. Krüger, N. Rösch, Inorg. Chim. Acta 363 (2010) 263.
[144] E. H. Bailey, J. F. W. Mosselmans, P. F. Schofield, Geochim. Cosmochim. Acta, 68 (2004) 1711.
[145] A. Kremleva, Y. Zhang, A. M. Shor, S. Krüger, C. Joseph, B. Radizky, K. Schmeide, S. Sachs, G. Bernhard, N. Rösch, submitted.
[146] S. Sachs, T. Reich, G. Bernhard, Radiochim. Acta 98 (2010) 467.
[147] C. Joseph, B. Raditzky, K. Schmeide, G. Geipel, G. Bernhard, in: Uranium Mining and Hydroteology, B. J. Merkel, A. Hasche-Berger (Eds.) Springer, Berlin, 2008, p. 539.
[148] S. Krüger, F. Schlosser, R. S. Ray, N. Rösch, in Lecture Series on Computer and Computational Sciences, vol. 7, T. Simonis, G. Maroulis (Eds.) Koninklijke Brill NV, Leiden, 2006, p. 904.
[149] F. Crea, A. De Robertis, S. Sammartano, Ann. Chim. 93 (2003) 1027.
[150] R. Portanova, P. Di Bernardo, A. Cassol, E. Tondello, L. Magon, Inorg. Chim. Acta 8 (1974) 233.
[151] A. Kirishima, Y. Onishi, N. Sato, O. Tochiyama, J. Chem. Thermodynam. 39 (2007) 1432.
[152] Ref. 2, vol. 4, chap. 23.6.
[153] H. Dong, H. Du, S. R. Wickramasinghe, X. Qian, J. Phys. Chem. B, 113 (2009) 14094.

[154] J. J. Berard, G. Schreckenbach, P. L. Arnold, D. Patel, J. B. Love, Inorg. Chem. 47 (2008) 11583.

[155] P. L. Arnold, D. Patel, A. Pécharman, C. Wilson, J. B. Love, Dalton Trans. 39 (2010) 3501.

[156] O. Zakharieva, A. Kremleva, S. Krüger, N. Rösch, Int. J. Quantum Chem. 211 (2011) 2045.

[157] C. Chiu, Density Functional Studies on Uranyl Complexation by Amino Acids, Bachelor Thesis, Technische Universität München, 2008.

[158] L. Rao, Chem. Soc. Rev. 36 (2007) 881.

[159] C. F. Baes, Jr., N. J. Meyer, Inorg. Chem. 1 (1962) 780.

[160] J. A. Hearne, A. G. White, J. Chem. Soc. (1957) 2168.

[161] P. Zanonato, P. Di Bernardo, A. Bismondo, G. Liu, X. Chen, L. Rao, J. Am. Chem. Soc. 126 (2004) 5515.

[162] L. Rao, A. Garnov, J. Jiang, P. Di Bernardo, P. Zanonato, A. Bismondo, Inorg. Chem. 42 (2003) 3685.

[163] L. Rao, J. Jiang, P. Zanonato, A. Bismondo, A. Garnov, Radiochim. Acta 90 (2002) 581.

[164] P. Di Bernardo, P. Zanonato, A. Bismondo, H. Jiang, A. Garnov, J. Jiang, L. Rao, Eur. J. Inorg. Chem. 22 (2006) 4533.

[165] T. G. Srinivasan, P. Zanonato, P. Di Bernardo, A. Bismondo, L. Rao, J. Alloys Compd. 408 (2006) 1252.

[166] L. Rao, P. Zanonato, P. Di Bernardo, J. Nucl. Radiochem. Sci. 6 (2005) 31.

[167] B. B. Owen, R. C. Miller, C. E. Milner, H. L. Cogan, J. Phys. Chem. 65 (1961) 2065.

[168] D. J. Bradley, K. S. Pitzer, J. Phys. Chem. 83 (1979) 1599.

[169] R. A. Pierotti, Chem. Rev. 76 (1976) 717.

[170] M. Cossi, B. Mennucci, R. Cammi, J. Comput. Chem. 17 (1996) 57.

[171] M. Cossi, V. Barone, R. Cammi, J. Tomasi, Chem. Phys. Lett. 255 (1996) 327.

[172] M. Tissandier, K. Cowen, W. Feng, E. Gundlach, M. Cohen, A. Earhart, J. Coe, J. Phys. Chem. A 102 (1998) 7787.

[173] S. Skanthakumar, M. R. Antonio, L. Soderholm, Inorg. Chem. 47 (2008) 4591.

[174] A. Ikeda-Ohno, C. Hennig, A. Rossberg, H. Funke, A. C. Scheinost, G. Berhanrd, T. Yaita, Inorg. Chem. 47 (2008) 8294.

[175] J.-M. Combes, C. J. Chisholm-Brause, G. E. Brown Jr., G. A. Parks, S. D. Conradson, P. G. Eller, I. R. Triay, D. E. Hobart, A. Meijer, Environ. Sci. Technol. 26 (1992) 376.

[176] K. Takao, S. Takao, A. C. Scheinost, G. Bernhard, C. Hennig, Inorg. Chem. 48 (2009) 8803.

[177] S. Tsushima, T. Yang, Chem. Phys. Lett. 401 (2005) 68.

[178] B. Brendebach, N. L. Banik, C. M. Marquardt, J. Rothe, M. A. Denecke, H. Geckeis, Radiochim. Acta 97 (2009) 701.

[179] A. Ikeda-Ohno, C. Hennig, S. Tsushima, A. C. Scheinost, G. Bernhard, T. Yaita, Inorg. Chem. 48 (2009) 7201.

[180] C. Hennig, J. Tutschku, A. Rossberg, G. Bernhard, A. C. Scheinost, Inorg. Chem. 44 (2005) 6655.

[181] H. Moll, M. A. Denecke, F. Jalilehvand, M. Sandström, I. Grenthe, Inorg. Chem. 38 (1999) 1795.

[182] S. Pocev, G. Johannson, Acta Chem. Scand. 27 (1973) 2146.

[183] M. R. Antonio, L. Soderholm, C. W. Williams, J. P. Blaudeau, B. E. Bursten, Radiochim. Acta 89 (2001) 17.

[184] P. G. Allen, J. J. Bucher, D. K. Shuh, N. M. Edelstein, I. Craig, Inorg. Chem. 39 (2000) 595.

[185] T. Stumpf, C. Hennig, A. Bauer, M. A. Denecke, T. Fanghänel, Radiochim. Acta 92 (2004) 139.

[186] S. Stumpf, T. Stumpf, K. Dardenne, C. Hennig, H. Foerstendorf, R. Klenze, T. Fanghänel, Environ. Sci. Technol. 40 (2006) 3522.

[187] Ref. 2, vol. 2, chap. 8.8.2c

[188] B. M. Thompson, P. A. Longmire, D. G. Brookings, Applied Geochem. 1 (1986) 335.

[189] Kristallin-I, Safety Assessment Report, Nagra Technical Reports NTB 93-22E, Nationale Genossenschaft für die Lagerung radioaktiver Abfälle, Wettingen Switzerland, 1994.

[190] A. Křepelová, S. Sachs, G. Bernhard, Radiochim. Acta 94 (2006) 825.

[191] C. J. Chisholm-Brause, J. M. Berg, K. M. Little, R. A. Matzner, D. E. Morris, J. Colloid Interface Sci. 277 (2004) 366.

[192] Z. M. Wang, J. M. Zachara, P. L. Gassman, C. X. Liu, O. Qafoku, W. Yantasee, J. G. Catalan, Geochim. Cosmochim. Acta 6 (2005) 1391.

[193] A. Křepelová, V. Brendler, S. Sachs, N. Baumann, G. Bernhard, Environ. Sci. Technol. 41 (2007) 6142.

[194] C. Hennig, T. Reich, R. Dähn, A. M. Scheidegger, Radiochim. Acta 90 (2002) 653.

[195] E. R. Sylwester, E. A. Hudson, P. G. Allen, Geochim. Cosmochim. Acta 64 (2000) 2431.

[196] A. Dent, J. D. F. Ramsay, S. W. Swanton, J. Colloid Interface Sci. 150 (1992) 45.

[197] A. Křepelová, T. Reich, S. Sachs, J. Drebert, G. Bernhard, J. Colloid Interface Sci. 319 (2008) 40.

[198] M. Schlegel, M. Descostes, Environ. Sci. Technol. 43 (2009) 8593.

[199] T. Hattori, T. Saito, K. Ishida, A. C. Scheinost, T. Tsuneda, S. Nagasaki, S. Tanaka, Geochim. Cosmochim. Acta 73 (2009) 5975.

[200] R. A. Young, A. W. Hewat, Clays Clay Miner. 36 (1988) 225.

[201] J. H. Lee, S. Guggenheim, Am. Miner. 66 (1981) 350.

[202] A. Kremleva, Environmental Chemistry of Uranyl: A Relativistic Density Functional Study on Complexation by Humic Substances and Sorption on Kaolinite, Doctoral Thesis, Technische Universität München, 2009.

[203] B. R. Bickmore, K. M. Rosso, K. L. Nagy, R. T. Cygan, C. J. Tadanier, Clays Clay Miner. 51 (2003) 359.

[204] P. Hartman, W. G. Perdok, Acta Crystallogr. 8 (1955) 49.

[205] P. Hartman, W. G. Perdok, Acta Crystallogr. 8 (1955) 521.

[206] P. Hartman, W. G. Perdok, Acta Crystallogr. 8 (1955) 525.

[207] I. D. Brown, D. Altermatt, Acta Cryst. B 41 (1985) 244.

[208] S. V. Churakov, J. Phys. Chem. B 110 (2006) 4135.

[209] S. V. Churakov, Geochim. Cosmochim. Acta 73 (2006) 1130.

[210] A. Kremleva, B. Martorell, S. Krüger. N. Rösch, Phys. Chem. Chem. Phys., DOI:10.1039/C2CP23886A.

[211] H. Thompson, G. Parks, J. Brown, in: Adsorption of Metals by Geomedia, E. Jenne (Ed.) Academic Press, San Diego, 1998, p. 350.

[212] T. Reich, R. Reich, S. Amayri, J. Drebert, N. L. Banik, R. A. Buda, J. V. Kratz, N. Trautmann, AIP Conf. Proc. 882 (2007) 179.

[213] T. Reich, G. Bernhard, G. Geipel, H. Funke, C. Hennig, A. Rossberg, W. Matz, N. Schell, H. Nitsche, Radiochim. Acta 88 (2000) 633.

[214] C. M. Marquardt (Ed.), Migration of actinides in the system clay, humic substances, aquifer, FZKA Rep. 7407, 2008.

[215] J. Catalano, G. E. Brown Jr., Geochim. Cosmochim. Acta 69 (2005) 2995.

[216] A. Kowal-Fouchard, R. Drot, E. Simoni, J. J. Erhardt, Environ. Sci. Technol. 38 (2004) 1399.

[217] A. Klamt, G. Schüürmann, J. Chem. Soc., Perkin Trans. 2 (1993) 799.

[218] J. L. Pascual-Ahuir, E. Silla, J. Comput. Chem., 12 (1990) 1047.

[219] J. L. Pascual-Ahuir, E. Silla, I. Tunon, J. Comput. Chem. 15 (1994) 1128.

[220] P. Su, H. Li, J. Chem. Phys. 130 (2009) 074109.

[221] A Ben-Naim, Y. Marcus, J. Chem. Phys. 81 (1984) 2016.

[222] R. S. Pearson, J. Am. Chem. Soc. 108 (1986) 6109.

[223] Y. Marcus, J. Chem. Soc. Faraday Trans. 87 (1991) 2995.

[224] R. Denning, in Gmelin Handbook of Inorganic Chemistry, Springer-Verlag, Berlin, 1983, U Suppl. Vol. A6, p. 46.

[225] H. H. Cornehl, C. Heinemann, J. Marcalo, A. P. de Matos, H. Schwarz, Angew. Chem. Int. Ed. Engl. 35 (1996) 891.

[226] M. Valiev, E. J. Bylaska, N. Govind, K. Kowalski, T. P. Straatsma, H.J.J. van Dam, D. Wang, J. Nieplocha, E. Apra, T. L. Windus, W. A. de Jong, Comput. Phys. Commun. 181 (2010) 1477.

[227] R. Ramakrishnan, A. V. Matveev, N. Rösch, Chem. Phys. Lett. 468 (2009) 158.

Berichtsblatt

1. ISBN oder ISSN	2. Berichtsart Abschlussbericht

3a. Titel des Berichts

Quantum Mechanical Modeling of Actinide Complexes: Complexation by Humic Substances and Sorption on Clay Minerals

3b. Titel der Publikation

4a. Autoren des Berichts (Name, Vorname(n)) Prof. Rösch, Notker; Dr. Krüger, Sven; Dr. Kremleva, Alena	5. Abschlussdatum des Vorhabens 30. 6. 2011
	6. Veröffentlichungsdatum
4b. Autoren der Publikation (Name, Vorname(n))	7. Form der Publikation
8. Durchführende Institution(en) (Name, Adresse) Technische Universität München Department Chemie, Theoretische Chemie Lichtenbergstr. 4 85748 Garching	9. Ber. Nr. Durchführende Institution
	10. Förderkennzeichen 02E10186
	11a. Seitenzahl Bericht 66
	11b. Seitenzahl Publikation
	12. Literaturangaben 227
13. Fördernde Institution (Name, Adresse) Bundesministerium für Wirtschaft und Technologie (BMWi) 53170 Bonn	14. Tabellen 21
	15. Abbildungen 15

16. Zusätzliche Angaben

17. Vorgelegt bei (Titel, Ort, Datum)

18. Kurzfassung

Das Projektes verfolgte zwei Ziele, die quantenmechanische Modellierung der Komplexierung von Actiniden durch natürliche Organika, insbesondere Huminstoffe, sowie erstmalig die Modellierung der Adsorption von Actiniden auf Tonmineralen auf diesem Niveau. Zur Berechnung relativistischer elektronischer und geometrischer Strukturen wurde die Dichtefunktionalmethode eingesetzt. Als Modelle für funktionelle Gruppen von Huminstoffen wurden verschiedene organische Moleküle verwendet. Tonmineraloberflächen wurden mit periodischen Schichtmodellen beschrieben. Für stickstoff- und schwefelhaltige funktionelle Gruppen konnte zusammen mit dem Experiment gezeigt werden, dass sie keine wesentliche Rolle bei der Actinidenkomplexierung durch Huminstoffe spielen. Die Modellierung ternärer Uranyl(VI)-Komplexe deutet auf eine schwächere Komplexierung von Hydrolysekomplexen im Vergleich zu freiem Uranyl hin. Die Temperaturabhängigkeit der Komplexierungskonstante von Uranylmono-acetat konnte auf eine bidentat gebundene Spezies zurückgeführt werden. Daneben wurden Americiumacetat sowie die Monohydroxide von U(IV) und Np(IV) rechnerisch charakterisiert. Die Modellierung der Adsorption von Uranyl(VI) auf Kaolinit, Pyrophyllit und einem Modellbeidellit sowie von Neptunyl(V) auf Kaolinit zeigten, dass von diversen adsorbierten Spezies auszugehen ist. Verschiedene Orientierung der Kantenflächen von Tonmineralen erlauben dabei verschiedene bevorzugte Adsorptionsplätze. Für bidentat koordinierte Komplexe wurden Geometrieparameter in Übereinstimmung mit EXAFS-Ergebnissen erhalten und eine Erweiterung der bisherigen Interpretation dieser Daten vorgeschlagen. Monodentate koordinierte sowie Hydrolyseprodukte können als adsorbierte Spezies ebenfalls vorkommen. Das Projekt wurde durch eine Verbesserung eines Solvatationsmodells für Komplexe in Lösung sowie die erstmalige Anwendung der DFT+U-Methode zur Korrektur von Selbst-wechselwirkungsfehlern bei Actiniden abgerundet.

19. Schlagwörter

Actinidenkomplexe, Aktinidenadsorption, Uran, Neptunium, Americium, Huminstoffe, Carboxylate, Sulfonate, Tonminerale, Kaolinit, Pyrophyllit, Quantenchemie, Dichtefunktionalmethode, Solvatation

20. Verlag	21. Preis

*) Auf das Förderkennzeichen des BMBF soll auch in der Veröffentlichung hingewiesen werden.

Document Control Sheet

1. ISBN or ISSN	2. Type of Report Final report

3a. Report Title

Quantum Mechanical Modeling of Actinide Complexes: Complexation by Humic Substances and Sorption on Clay Minerals

3b. Title of Publication

4a. Author(s) of the Report (Family Name, First Name(s)) Prof. Rösch, Notker; Dr. Krüger, Sven; Dr. Kremleva, Alena	5.End of Project 30. 6. 2011
	6. Publication Date
4b. Author(s) of the Publication (Family Name, First Name(s))	7. Form of Publication
8. Performing Organization(s) (Name, Address) Technische Universität München Department Chemie, Theoretische Chemie Lichtenbergstr. 4 85748 Garching	9. Originator's Report No.
	10. Reference No. 02E10186
	11a. No. of Pages Report 66
	11b. No. of Pages Publication
13. Sponsoring Agency (Name, Address) Bundesministerium für Wirtschaft und Technologie (BMWi) 53170 Bonn	12. No. of References 227
	14. No. of Tables 21
	15. No. of Figures 15

16. Supplementary Notes

17. Presented at (Title, Place, Date)

18. Abstract

The two central goals of the project were the quantum mechanical modeling of the complexation of actinides by natural organic matter, in particular by humic substances, and, for the first time, the modeling of actinide adsorption on clay minerals on that level of theory. Relativistic electronic and geometric structures have been calculated with a density functional approach. Small organic molecules were used as models of functional groups of humic substances. Periodic slabs were applied to model surfaces of clay minerals. Together with experiment it was shown that functional groups containing nitrogen or sulfur play only a minor role for actinide complexation by humic substances. Results on ternary uranyl(VI) complexes point toward a weaker complexation of hydrolysis products compared to free actinide ions. The temperature dependence of the complexation constant of uranyl monoacetate were traced back to a bidentate coordinated species. Besides these results, also americium acetate and U(IV) and Np(IV) monohydroxide have been characterized. Model calculations of the adsorption of uranyl(VI) on kaolinite, pyrophyllite, and a model beidellite, as well as of neptunyl(V) on kaolinite showed that various adsorbed species should be present. Different orientations of edge surfaces of clay minerals may provide different preferred adsorption sites. For bidentate coordinated adsorbed actinide species geometry parameters in agreement with EXAFS results were calculated and an extension of the current interpretation of these data was suggested. Besides, also monodentate coordinated species as well as hydrolysis products are possible adsorbed complexes. Work on the project also comprised an improved solvation model for complexes in solution and the first application of the DFT+U method to actinide complexes for the correction of self-interaction artifacts.

19. Schlagwörter

actinide complexes, actinide adsorption, uranium, neptunium, americium, humic substances, carboxylate, sulfonate, clay minerals, kaolinite, pyrophyllite, quantum chemistry , density functional method, solvation

20. Publisher	21. Price